Free Radical Biology and Medicine 108 (2017) 904–917

Contents lists available at ScienceDirect

Free Radical Biology and Medicine

journal homepage: www.elsevier.com/locate/freeradbiomed

Original article

Non-thermal plasma induces a stress response in mesothelioma cells resulting in increased endocytosis, lysosome biogenesis and autophagy

Lei Shi[a], Fumiya Ito[a], Yue Wang[a], Yasumasa Okazaki[a], Hiromasa Tanaka[b], Masaaki Mizuno[b], Masaru Hori[c], Tasuku Hirayama[d], Hideko Nagasawa[d], Des R. Richardson[e,*], Shinya Toyokuni[a,e,**]

[a] Department of Pathology and Biological Responses, Nagoya University Graduate School of Medicine, Nagoya 466-8550, Japan
[b] Center for Advanced Medicine and Clinical Research, Nagoya University Hospital, Nagoya 466-8550, Japan
[c] Plasma Nanotechnology Research Center, Nagoya University, Nagoya 464-8603, Japan
[d] The Laboratory of Pharmaceutical and Medicinal Chemistry, Gifu Pharmaceutical University, Gifu, Japan
[e] Molecular Pharmacology and Pathology Program, Department of Pathology and Bosch Institute, The University of Sydney, Sydney, NSW 2006, Australia

ARTICLE INFO

Keywords:
Non-thermal plasma
Cancer
Autophagy
Lysosome
Iron

ABSTRACT

Non-thermal plasma (NTP) is a potential new therapeutic modality for cancer. However, its mechanism of action remains unclear. Herein, we studied the effect of NTP on mesothelioma cells and fibroblasts to understand its anti-proliferative efficacy. Interestingly, NTP demonstrated greater selective anti-proliferative activity against mesothelioma cells relative to fibroblasts than cisplatin, which is used for mesothelioma treatment. The anti-proliferative effect of NTP was enhanced by pre-incubation with the cellular iron donor, ferric ammonium citrate (FAC), and inhibited by iron chelation using desferrioxamine (DFO). Three oxidative stress probes (CM-H2DCFDA, MitoSOX and C11-BODIPY) demonstrated reactive oxygen species (ROS) generation by NTP, which was inhibited by DFO. Moreover, NTP decreased transferrin receptor-1 and increased ferritin-H and -L chain expression that was correlated with decreased iron-regulatory protein expression and RNA-binding activity. This regulation was potentially due to increased intracellular iron in lysosomes, which was demonstrated *via* the Fe (II)-selective probe, HMRhoNox-M, and was consistent with autophagic-induction. Immunofluorescence using LysoTracker and Pepstatin A probes demonstrated increased cellular lysosome content, which was confirmed by elevated LAMP1 expression. The enhanced lysosomal biogenesis after NTP could be due to the observed increase in fluid-phase endocytosis and early endosome formation. These results suggest NTP acts as a stressor, which results in increased endocytosis, lysosome content and autophagy. In fact, NTP rapidly increased autophagosome formation, as judged by increased LC3B-II expression, which co-localized with LAMP1, indicating autophago-lysosome formation. Autophagic-induction by NTP was confirmed using electron microscopy. In summary, NTP acts as a cellular stressor to rapidly induce fluid-phase endocytosis, lysosome biogenesis and autophagy.

1. Introduction

Malignant mesothelioma is a rare, but highly aggressive cancer in humans that occurs after exposure to asbestos [1,2]. The average survival time after initial diagnosis was 13.7 months in 1992 [3] and has not significantly improved after several decades [4]. The pathogenesis of the disease involves the inhalation of asbestos fibers that damage the mesothelial cells lining the somatic cavity. The most likely mechanism of asbestosis carcinogenicity involves both direct and indirect genotoxicity [1,5–7]. Direct genotoxicity involves the penetration of cells by asbestos fibers, which can result in DNA strand breaks, micronuclei formation and aneuploidy [6,8,9]. Indirect genotoxic activity can result from the ability of asbestos fibers to generate reactive oxygen species (ROS) [10], which may be facilitated by increased local iron levels [11–13].

Furthermore, it has been demonstrated in laboratory studies using

Abbreviations: AKT, activation of oncogenic protein kinase; AL, autophagolysosome; AP, autophagosome; ATM, ataxia-telangiectasia mutated; ATR, ATM- and Rad3-related; BSA, bovine serum albumin; CTRL, control; DAPI, 4′,6-diamidino-2-phenylindole; DFO, desferrioxamine (desferal); EEA1, early endosome antigen 1; FAC, ferric ammonium citrate; FtL, ferritin light chain; FtH, ferritin heavy chain; HBSS+, Hanks' balanced salt solution with calcium and magnesium; IRP, iron-regulatory protein; IRE, iron-responsive element; LAMP1, lysosomal-associated membrane protein 1; LC3B, microtubule-associated protein 1 light chain 3 beta; MUL1, mitochondrial E3 ubiquitin protein kinase 1; NTP, non-thermal plasma; PAS, pre-autophagic structure; PBS, phosphate-buffered saline; ROS, reactive oxygen species; RT, room temperature; TfR1, transferrin receptor 1; TFEB, transcription factor EB

* Corresponding and senior author.
** Corresponding and senior author at: Department of Pathology and Biological Responses, Nagoya University Graduate School of Medicine, Nagoya, Japan.
E-mail addresses: d.richardson@med.usyd.edu.au (D.R. Richardson), toyokuni@med.nagoya-u.ac.jp (S. Toyokuni).

http://dx.doi.org/10.1016/j.freeradbiomed.2017.04.368
Received 16 December 2016; Received in revised form 19 April 2017; Accepted 28 April 2017
Available online 02 May 2017

animals that the administration of a redox-active iron chelator accelerated mesothelioma development induced by asbestos exposure [14]. Interestingly, the chromosomal aberrations that are mediated by asbestos fibers can be counteracted by redox-inactive iron chelators and ROS scavengers/antioxidants [15,16]. These latter studies with the recently developed ligand, deferasirox, underline the role of iron and oxidative stress in the pathogenesis of malignant mesothelioma [13,17,18].

Currently, the treatment of malignant mesothelioma involves the combination of surgery, chemotherapy (including folate antagonists and platinum-based drugs, such as cisplatin) and radiotherapy [19,20]. However, success with these therapeutic regimens has been dismal, strongly demonstrating the need for new and effective treatments [21]. An interesting new form of therapy involves the generation of non-thermal plasma (NTP) [22–24]. NTP is a partially ionized gas in which energy is stored predominantly as free electrons and the temperature remains as low as body temperature [25,26]. For many years, NTP has been used in a variety of applications, such as low-temperature plasma chemistry and the removal of gaseous pollutants [27,28]. However, in more recent years, the use of NTP has expanded to prion inactivation and biomedical applications, where it may have potential for the treatment of septic wounds and cancer [29,30].

Recent studies have demonstrated that NTP shows antitumor activity *in vitro* against a range of tumor cell-types, including glioblastoma, colorectal carcinoma, melanoma, breast cancer and hepatocellular carcinoma, *via* the induction of DNA damage, cell cycle arrest and apoptosis [22,31,32]. Interestingly, DNA damage resulting from the treatment of cells with NTP activates cellular signaling through the activation of ataxia-telangiectasia mutated and Rad3-related (ATR) to phosphorylate the histone variant H2AX in the vicinity of the DNA damage [25]. We recently showed that NTP exposure can cause not only single- and double-strand DNA breaks, but also base modifications and pyrimidine dimers [33].

Studies *in vivo* in mice bearing glioblastoma xenografts have demonstrated that NTP decreased tumor volume, increased lifespan and resulted in an accumulation of cells in the S phase of the cell cycle [22,34,35]. Furthermore, using syngeneic and xenograft head and neck tumor models, NTP resulted in a decrease in tumor size and a reduction in the activation of oncogenic protein kinase B (AKT), which may be due to increased mitochondrial E3 ubiquitin protein kinase 1 (MUL1) expression [23,36].

While the cellular response to NTP in terms of ROS generation, cell cycle arrest and apoptosis has been characterized, the role of iron, ROS and autophagy in terms of the biological efficacy of NTP has not been assessed. This is important to evaluate, considering that iron can potentiate ROS generation, and thus, tumor cell killing. The current investigation demonstrates for the first time that NTP is selectively cytotoxic to mesothelioma cells and induces a cellular stress response probably mediated *via* iron-induced ROS generation. This response consists of a marked increase in fluid-phase endocytosis/pinocytosis, early endosome formation, lysosome biogenesis and autophagy. The pronounced induction of autophagy by NTP is important in terms of understanding the cellular mechanism of action of this new treatment modality.

2. Materials and methods

2.1. Materials

Cells were grown in 96-well plates and 60 mm dishes (Thermo Fisher Scientific, Waltham, MA). Ferric ammonium citrate (FAC) and desferrioxamine (DFO) were purchased from Sigma-Aldrich (St. Louis, MO).

2.2. Cell culture

The human fibroblast cell line IMR 90SV was obtained from the Riken Cell Bank (Ibaraki, Japan) and Rat-1, a rat fibroblast cell line, was from Riken BRC (Tsukuba, Japan). The rat SM2 (sarcomatoid sub-type) and EM2 (epithelioid sub-type) malignant mesothelioma cells were established from rats injected with asbestos using an established protocol [14]. All the cells were grown in RPMI-1640 medium (Wako, Osaka, Japan) containing 10% fetal bovine serum (Biowest, Nuaillé, France) and 1% antibiotic-antimycotic solution (Invitrogen, Carlsbad, CA), hereafter referred to as complete medium. The cells were maintained at 37 °C in a humidified incubator at 5% CO_2.

2.3. Non-thermal plasma

NTP was generated by following a well-established procedure [37] using a Hababiro (wide orifice) instrument (from Prof. M. Hori, Plasma Nanotechnology Research Center, Nagoya University, Nagoya, Japan) by applying 10 kV from a 60 Hz commercial power supply using 2 electrodes that were 20 mm apart. The NTP was of ultra-high electron density (approximately 2×10^{16} cm^{-3}) that had an O density of approximately 4×10^{15} cm^{-3}, as previously reported [35]. Argon was used as the gas for generating NTP and implemented at a flow rate of 2 L/min, and the distance between the plasma source and samples was fixed at L = 8 mm. In all the experiments, cells in complete media were treated with NTP for 30–120s/25 °C and then returned to 37 °C for various incubation periods. For studies using 96-well plates, a cover was utilized to treat each well. As a relevant control, studies were performed using Argon alone under the same experimental conditions.

2.4. Cell viability assay

In these studies, 5000 cells/well were seeded in 96-well plates (Cat. #167008, Thermo Fisher Scientific) and incubated for 24 h/37 °C. The cells were then treated with NTP for 30–120 s/25 °C. After a 24 h/37 °C incubation in complete medium, the cell count reagent SF (Cat. #07553 Nacalai Tesque, Kyoto, Japan) was used to determine the viability of the cells after treatment with NTP.

2.5. Analysis of reactive oxygen species production

General oxidative stress in cells was assessed using the chloromethyl derivative of 2′,7′-dichlorodihydrofluorescein diacetate (CM-H_2DCFDA; Cat. #c6827, Thermo Fisher Scientific). Mitochondrial superoxide was assessed using MitoSOX (Cat. #M36008, Thermo Fisher Scientific), and lipid peroxidation was detected by BODIPY 581/591 C11 (Cat. #D3861, Thermo Fisher Scientific). Cells were treated with NTP and after 0.5 h/37 °C were stained with either CM-H_2DCFDA (10 μM), MitoSOX (5 μM), or BODIPY 581/591 C11 (2 μM) in HBSS(+) for 0.5 h. The cells were then collected and analyzed using flow cytometry (Gallios BD, Beckman Coulter, Brea, CA) to detect ROS and lipid peroxidation.

2.6. Protein extraction and immunoblotting

Before treatment with NTP, mesothelioma cells (2.5×10^5) or IMR 90SV fibroblasts (1×10^6) were plated onto 60-mm dishes and incubated for 48 h/37 °C. After treatment with NTP at different doses, cells were then incubated for 24 h/37 °C in complete medium and subsequently collected and lysed to extract proteins. The primary antibodies used for immunoblotting were against transferrin receptor 1 (Cat. #clone H64.8; 1/500 dilution; Invitrogen), ferritin heavy (H) chain (Cat. #sc-25617; 1/200 dilution; Santa Cruz Biotechnology, Dallas, TX), ferritin light (L) chain (Cat. #ab69090; 1/1000 dilution; Abcam, Cambridge, UK), LAMP1 (Cat. #ab25630; 1/200 dilution), and LC3B (Cat. #D11, 1/1000 dilution; Cell Signaling Technology, Danvers, MA.

In studies assessing the expression of the transcription factor EB (TFEB), nuclear and cytoplasmic fractions were collected after centrifugation (200 x g/5 min/4 °C), and an antibody against TFEB (Cat. #13372, Proteintech, Rosemont, IL; 1/1000 dilution) used for immunoblotting. Antibodies against β-actin (Cat. #clone AC-15; 1/2000 dilution; Sigma) and lamin B (Cat. #sc-6217, Santa Cruz Biotechnology; 1/300 dilution) were used as protein-loading controls for the cytoplasmic and nuclear fractions, respectively.

2.7. Iron Regulatory Protein (IRP)-Iron-Responsive Element (IRE)–binding: native gel shift assay

To assess IRP-IRE-binding activity, a Light Shift Chemiluminescent RNA EMSA Kit was used according to the protocol provided by the manufacturer (Cat. #77016, Thermo Fisher Scientific). Briefly, cytosolic cell extracts (1.5 μg) were incubated with biotinylated IRE-RNA in 1× binding buffer, 5% (v/v) glycerol, 0.1 mg/mL *t*RNA, and nuclease-free water in a total volume of 20 μL at room temperature (RT) for 20 min. The mixture was then electrophoresed on 6% (w/v) non-denaturing polyacrylamide gels in 0.5× TBE buffer at 150 V for 3 h. The transfer was performed using biodyne B nylon membranes and a semi-dry transfer apparatus. The transferred RNA was cross-linked to the membranes with a UV transilluminator for 5 min at RT. To detect biotinylated RNA with chemiluminescence, the Chemiluminescent Nucleic Acid Detection Module (Cat. #89880, Thermo Fisher Scientific) was used.

2.8. Immunofluorescence using confocal microscopy

After SM2 cells were treated with NTP for 60 s, they were then incubated for 2, 4, or 8 h/37 °C. The cells were then fixed with 4% (w/v) paraformaldehyde for 10 min/RT, washed 3 times using PBS, incubated with 0.1% (v/v) Triton X100 and blocked for 1 h at RT with 3% (w/v) BSA. The cells were then incubated overnight at 4 °C with primary antibodies against LAMP1 (Cat. #ab25630; 1/2000 dilution; Abcam) or LC3B (Cat. #D11; 1/1000 dilution; Cell Signaling Technology), washed 3 times with PBS and incubated with the secondary antibodies, CF™488A and CF™568 (Biotium, Inc., Fremont, CA), respectively. A Zeiss confocal microscope (LSM880, Carl Zeiss, Oberkochen, Germany) was used to observe cellular morphology. The fluorescence intensity and Mander's overlap for image co-localization were measured using ImageJ 4.7v software (National Institutes of Health, Bethesda, MD). Fifty cells were quantified with ImageJ software for integration of each fluorescence (wavelength) area *via* excluding the cellular background. The relative intensity per cell in arbitrary units is shown.

2.9. Catalytic Fe(II) imaging

HMRhoNox-M, a catalytic Fe(II)-specific probe, was synthesized and characterized, as described [38]. In these studies, 2×10^4 SM2 cells were plated into glass bottom dishes (Cat. #D11131H, Matsunami, Osaka, Japan) and incubated overnight. After treatment with NTP (60 s), the cells were incubated for 0.5 h/37 °C with HMRhoNox-M (10 μM) in HBSS(+) and LysoTracker Green DND99 (Cat. #L7528, ThermoFisher Scientific) simultaneously (200 nM). The cells were then washed 3 times with HBSS(+) and imaged using the confocal microscope described above. The cells were then stained with Hoechst 33342 (Cat. #H1399, Thermo Fisher Scientific) and counted.

2.10. Assessment of lysosomal membrane permeability and lysosomal content

Live cell imaging with the confocal microscope described above was used to detect lysosomal content by observing a potent inhibitor of lysosomal enzymes, pepstatin A, using BODIPY FL-pepstatin A (Cat. #P12271; Thermo Fisher Scientific). SM2 cells were treated with or without NTP for 60 s and subsequently incubated for 4 h/37 °C. The cells were then stained with BODIPY FL-pepstatin A (10 μM) for 30 min and also with Hoechst 33342 (1 μg/mL).

2.11. Fluid-phase endocytosis and early endosome marker analysis

Cells were incubated with the fluid-phase endocytosis marker, pHrodo Red Dextran (10 μg/mL; P10361, Thermo Fisher Scientific) [39] in medium and treated with NTP for 60 s. After an incubation for 0, 2, 4 or 8 h, the cells were then fixed and incubated with an antibody against the well-characterized early endosomal marker, EEA1 [40] (Cat. #610457, BD BioSciences Pharmingen, San Diego, CA; 1:1000) at 4 °C overnight. After 3 washes with PBS and then incubation with the secondary antibody, CF™488A, the Zeiss confocal microscope above was used to observe cellular morphology. The fluorescence intensity and Mander's overlap coefficient for image co-localization were measured using ImageJ 4.7v software.

2.12. Transmission electron microscopy

SM2 cells were treated with or without NTP (60 s) and then incubated for 6 h/37 °C. Then, glutaraldehyde (2 mM) in PBS (1 mM) was used to fix the samples, implementing standard protocols [41]. Transmission electron microscopy using a JEM-1400PLUS (JEOL, Tokyo, Japan) instrument was then performed.

2.13. Statistical analysis

The results were expressed as the mean ± standard error of the mean (SEM; 3 experiments). The statistical analysis was performed using Student's *t*-test and two-way ANOVA (Bonferroni post-hoc test) with GraphPad Prism 5 software (GraphPad Software, La Jolla, CA).

3. Results

3.1. NTP demonstrates selective anti-proliferative activity against malignant mesothelioma cells relative to a non-tumorigenic fibroblast cell line

Previous studies have assessed the anti-proliferative activity of NTP against various cancer cell-types *in vitro* relative to normal cells [32,42,43]. To assess the efficacy and selectivity of NTP, our initial experiments examined the activity of NTP relative to the commonly used cytotoxic agent, cisplatin, in malignant mesothelioma cells (SM2 and EM2) relative to a non-tumorigenic fibroblast cell line [44] (IMR 90SV; Fig. 1**Ai**). Notably, cisplatin was used as an appropriate reference chemotherapeutic, as it is widely used for the treatment of malignant mesothelioma [45].

Cisplatin demonstrated little selective activity against malignant mesothelioma cells relative to the fibroblast cell line after a 24-h incubation (Fig. 1**Ai**). In fact, the IC_{50} of cisplatin in both malignant mesothelioma cells (*i.e.*, EM2 cells: 3.4 ± 1.5 μM; SM2 cells: 10.0 ± 1.2 μM) was within the range found for the IMR 90SV fibroblast cell line (9.9 ± 1.2 μM).

In studies using NTP, the cells were treated in complete medium for 30–120 s with NTP prior to a 24-h incubation, after which, cellular proliferation was assessed (Fig. 1**Aii**). This treatment protocol with NTP enabled an appropriate dosage schedule to assess its anti-proliferative efficacy, which was time-dependent, and permitted the comparison to previous studies examining the activity of NTP against non-neoplastic cells [33]. In contrast to cisplatin, NTP demonstrated greater selective ($p < 0.001$) anti-proliferative activity after treatment times of 60, 90 and 120 s against both malignant mesothelioma cell lines relative to the IMR 90SV fibroblast cell line (Fig. 1**Aii**). We obtained similar results using the rat fibroblast cell line, Rat-1, which was significantly ($p < 0.001$) more resistant to the anti-proliferative activity of NTP than

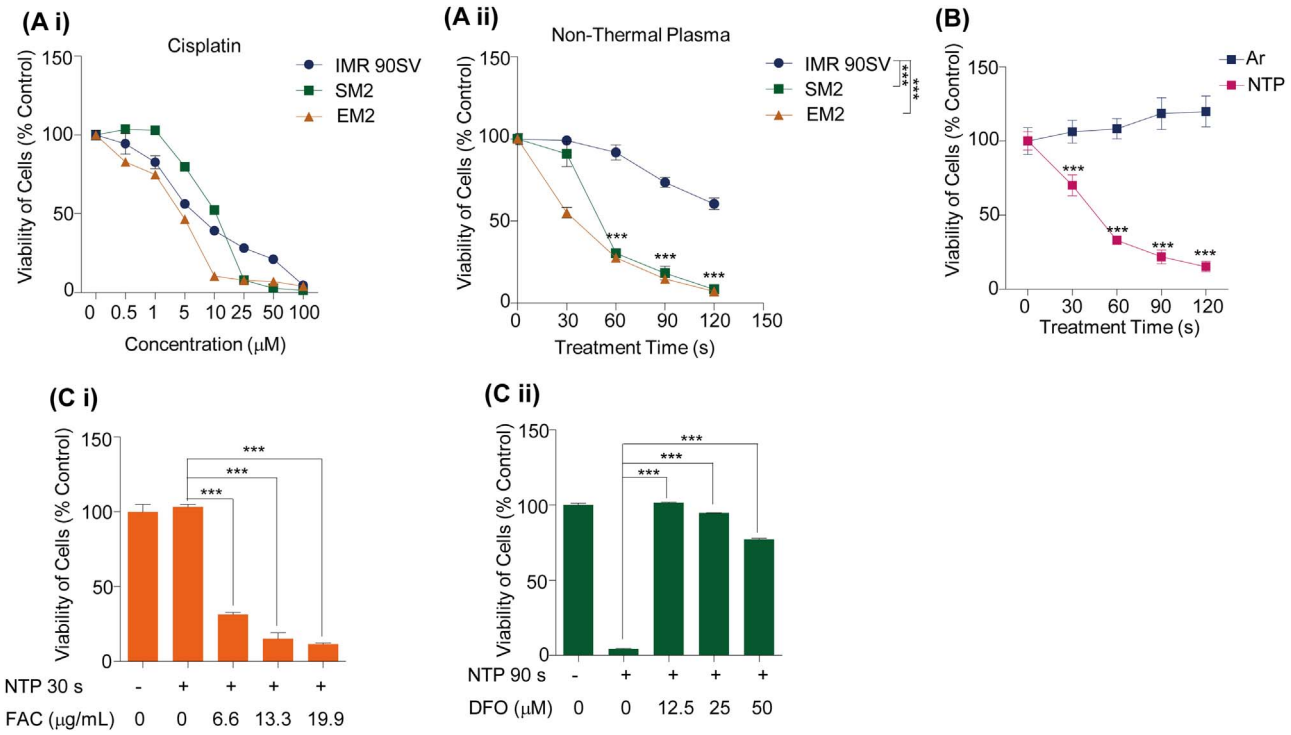

Fig. 1. Non-thermal plasma (NTP) demonstrates selective, iron-dependent anti-proliferative activity against malignant mesothelioma cells relative to fibroblasts. (Ai, ii) IMR 90SV human lung fibroblast cells and SM2 (sarcomatoid sub-type) and EM2 (epithelioid sub-type) rat malignant mesothelioma cells were treated with cisplatin (0.5–100 μM) or NTP (30–120 s), and the cell viability was examined after an incubation of 24 h/37 °C. **(B)** SM2 cells were treated with argon (Ar; control) or NTP (30–120 s), and the cell viability was assessed after an incubation of 24 h/37 °C. **(Ci)** SM2 cells were loaded with iron during a 3 h/37 °C pre-incubation with the cellular Fe donor, ferric ammonium citrate (FAC; 6.6, 13.3, or 19.9 μg/mL), in complete medium. The cells were then treated with NTP for 30 s, and the incubation continued in the same medium for 24 h/37 °C. The viability was then assessed. **(Cii)** SM2 cells were pre-incubated for 3 h/37 °C with or without DFO (12.5, 25 and 37.5 μM) in complete medium and then treated with NTP for 90 s, and the incubation continued in the same medium for 24 h/37 °C. The cellular viability was then examined. The results are shown as the mean ± SEM ($n = 3$). ***, $p < 0.001$ *vs.* control.

the SM2 and EM2 mesothelioma cell lines after 60, 90 and 120 s (Supplementary Fig. S1). Hence, non-neoplastic cells were less sensitive to the anti-proliferative effects of NTP than neoplastic cells. As a relevant control for NTP treatment, which involves the use of argon gas, SM2 cells were treated with the same argon stream under identical experimental conditions, but without electrical activation. Notably, argon alone had no significant ($p > 0.05$) effect on cellular proliferation (Fig. 1**B**).

In conclusion, these *in vitro* studies support the use of NTP as a potential selective therapeutic strategy against malignant mesothelioma cells.

3.2. Contrasting effects of iron-loading and -depletion on the anti-proliferative efficacy of NTP against malignant mesothelioma cells

Considering the selective anti-proliferative effect of NTP on malignant mesothelioma cells (Fig. 1**Aii**), studies were designed to understand the mechanism of this activity. Previous studies have indicated that the major biological effector of the anti-proliferative activity of NTP is ROS generation [32,46]. As cellular iron levels can potently mediate and accelerate the toxicity of ROS *via* Fenton/Haber-Weiss chemistry [47,48], studies were designed to assess the effects of cellular iron-loading and -depletion on the anti-proliferative efficacy of NTP using the SM2 mesothelioma cells (Fig. 1**C(i, ii)**).

In these studies, SM2 cells were loaded with iron during a 3 h/37 °C pre-incubation with a well-characterized cellular Fe donor, ferric ammonium citrate (FAC; 6.6, 13.3, or 19.9 μg/mL) [49], in complete medium. The cells were then treated with NTP for 30 s, and the incubation continued in the same medium for 24 h/37 °C (Fig. 1**Ci**). Notably, the studies in Fig. 1**Aii** demonstrated that treatment of SM2 cells with 30 s of NTP did not lead to marked anti-proliferative efficacy after 24 h. Hence, this sub-optimal NTP dose was used to assess if FAC could potentiate its anti-proliferative efficacy (Fig. 1**Ci**). In fact, pre-incubation with FAC (at 6.6, 13.3, or 19.9 μg/mL) resulted in a marked and significant ($p < 0.001$) increase in the anti-proliferative efficacy of NTP.

Considering that cellular iron-loading potentiated the activity of NTP, studies were then designed to investigate the effect of iron-depletion using the redox-inactive and clinically implemented "gold standard" chelator, DFO (12.5–37.5 μM), that is known to decrease cellular iron levels [49,50]. In these studies, cells were pre-incubated for 3 h/37 °C with or without DFO (12.5, 25 and 37.5 μM) in complete medium and then treated with NTP for 90 s, and the incubation continued in the same medium for 24 h/37 °C (Fig. 1**Cii**). A 90 s treatment with NTP was determined, as shown in Fig. 1**Aii,** to result in marked anti-proliferative activity, and therefore, the effect of DFO in preventing this response was tested. Interestingly, incubation with DFO at all concentrations tested markedly and significantly ($p < 0.001$) prevented the anti-proliferative activity of NTP (Fig. 1**Cii**). In fact, DFO at a concentration of 12.5 μM totally inhibited the anti-proliferative activity of NTP. The observed decrease in cellular viability that occurred with increasing DFO levels in the presence of NTP was probably due to the ability of the chelator to bind intracellular iron [51] and inhibit growth and viability (Fig. 1**Cii**).

In summary, these studies with FAC and DFO demonstrate that cellular iron plays a significant role in the anti-proliferative activity of NTP in malignant mesothelioma cells.

3.3. Treatment of malignant mesothelioma cells with NTP results in iron-dependent intracellular ROS generation

Considering the marked effect of DFO in inhibiting the anti-proliferative activity of NTP (Fig. 1**C**), studies were designed to examine the NTP-mediated ROS generation after incubation with this chelator

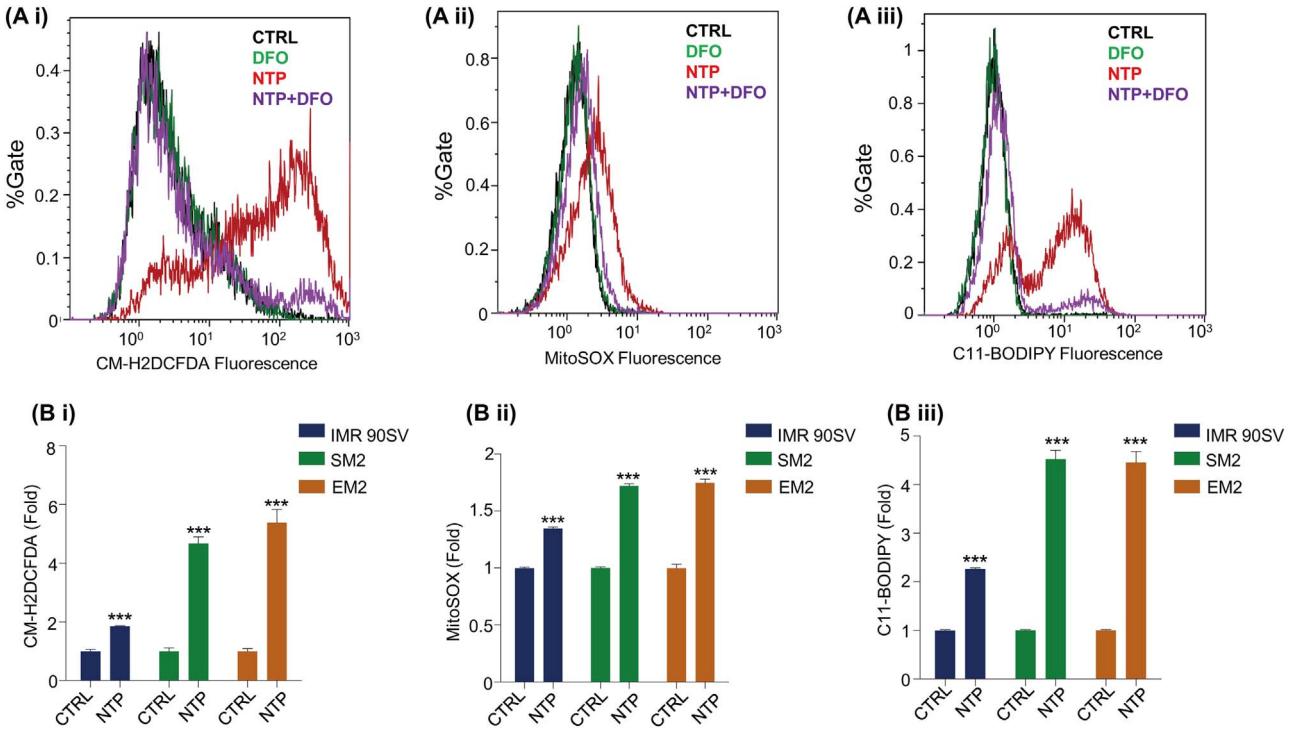

Fig. 2. NTP results in iron- and cell-type-dependent ROS generation. (Ai–iii) SM2 malignant mesothelioma cells were treated with NTP (60 s) with or without a pre-incubation with DFO (12.5 μM) for 3 h/37 °C. The cells were then incubated for an additional 30 min/37 °C in the absence of DFO, and ROS generation was detected by flow cytometry using the probes CM-H2DCFDA, MitoSOX, or C11-BODIPY. **(Bi–iii)** IMR 90SV cells, SM2 cells and EM2 cells were treated with or without NTP (60 s) and then incubated for an additional 30 min/37 °C, and ROS generation was determined using the probes CM2-DCFDA, MitoSOX, or C11-BODIPY. The data in **Ai, ii, iii** are typical flow cytometry profiles from 3 experiments. **Bi–iii** are shown as the mean ± SEM ($n = 3$). ***, $p < 0.001$ *vs.* control.

(Fig. 2**Ai–iii**). To assess intracellular ROS generation, three well-characterized redox-sensitive probes were utilized, namely, CM-H_2DCF-DA (10 μM; Fig. 2**Ai**), MitoSOX (5 μM; Fig. 2**Aii**) and C11-BODIPY (2 μM; Fig. 2**Aiii**) [52–54].

In these studies, SM2 cells were pre-incubated with complete medium or medium containing DFO (12.5 μM) for 3 h/37 °C and then treated with NTP for 60 s. The incubation of the cells was then continued for 30 min/37 °C (Fig. 2**Ai–iii**). A 60 s-dose of NTP was utilized because it caused significant cytotoxicity, but not complete cellular ablation. Thus, this protocol enabled the measurement of cellular ROS. The cells were then collected and incubated with either of the 3 redox-sensitive probes and flow cytometric analysis then performed (Fig. 2**Ai–iii**). Incubation with DFO alone did not markedly affect the cytometric profiles relative to control (CTRL) cells. However, for all three probes, treatment with NTP resulted in a change in the cytometric profile, indicating ROS generation in the cells. This effect was markedly prevented by pre-incubation with the chelator, DFO (NTP + DFO), suggesting the role of iron in NTP-generated ROS (Fig. 2**Ai–iii**). Notably, for both H2DCFDA and C11-BODIPY, treatment of cells with NTP resulted in a marked 8–16-fold increase in the oxidation of the probe relative to the CTRL cells (Fig. 2**Ai, iii**), whereas for MitoSOX, there was only a 2-fold increase (Fig. 2**Aii**).

It may be suggested that the differential ROS-induced oxidation of the probes could be affected by their intracellular compartmentalization, which has been reported for these agents. In fact, CM-H_2DCFDA has been reported to detect cytoplasmic ROS [55], MitoSOX is thought to detect mitochondrial ROS [56], and C11-BODIPY assesses membrane lipid peroxidation [57]. Overall, these studies demonstrate that NTP results in the iron-dependent generation of ROS in cells. Furthermore, considering these results, a 60 s-dose of NTP was used for all subsequent studies, as it was sufficiently active, but maintained cellular viability at a level that allowed subsequent analysis.

3.4. Cell-type-dependent sensitivity to NTP is associated with intracellular ROS generation

Next, the studies in Fig. 2**Bi** then assessed the effect of a 60 s-dose of NTP (NTP 60 s) on ROS generation in the malignant mesothelioma cell lines (SM2 and EM2) that were sensitive to NTP relative to the more resistant fibroblast cell-type (IMR 90SV; Fig. 1**Aii**). Notably, among these 3 cell-types, the IMR 90SV fibroblast cell line demonstrated the lowest fold-change (1.3–2-fold) in the generation of ROS by NTP relative to the CTRL for the 3 redox-sensitive probes, CM-H_2DCFDA (Fig. 2**Bi**), MitoSOX (Fig. 2**Bii**) and C11-BODIPY (Fig. 2**Biii**). In contrast, for both the SM2 and EM2 malignant mesothelioma cell lines, the fold change in ROS generation after incubation with NTP relative to the CTRL was significantly ($p < 0.001$) greater for each individual probe than that found for the fibroblasts (Fig. 2**Bi–iii**). Again, for each cell-type, it was shown that the fold-change between the CTRL and NTP-treated cells was least for the MitoSOX probe (Fig. 1**Bii**). Collectively, these studies in Figs. 1**Aii** and 2**Bi–iii** demonstrate the positive relationship between the sensitivity of cells to the anti-proliferative activity of NTP and the generation of cellular ROS.

3.5. NTP decreased IRP1/2 and TfR1 expression and increased ferritin-H/L levels

The studies above demonstrate that the cellular Fe donor, FAC, can potentiate the anti-proliferative activity of NTP (Fig. 1**Ci**). In contrast, the iron chelator, DFO, can offset the anti-proliferative activity of NTP (Fig. 1**Cii**) and prevent its ability to induce ROS (Fig. 2**Ai–iii**). Considering this, these studies indicate a role for iron in the efficacy of NTP. Hence, our experiments then assessed the effect of NTP on the expression of proteins involved in iron metabolism, as these could be influenced by this treatment and play a role in its mechanism of action (Fig. 2**A**). Immunoblotting was used to first assess the expression of IRP1 and IRP2, which are major regulators of iron metabolism through

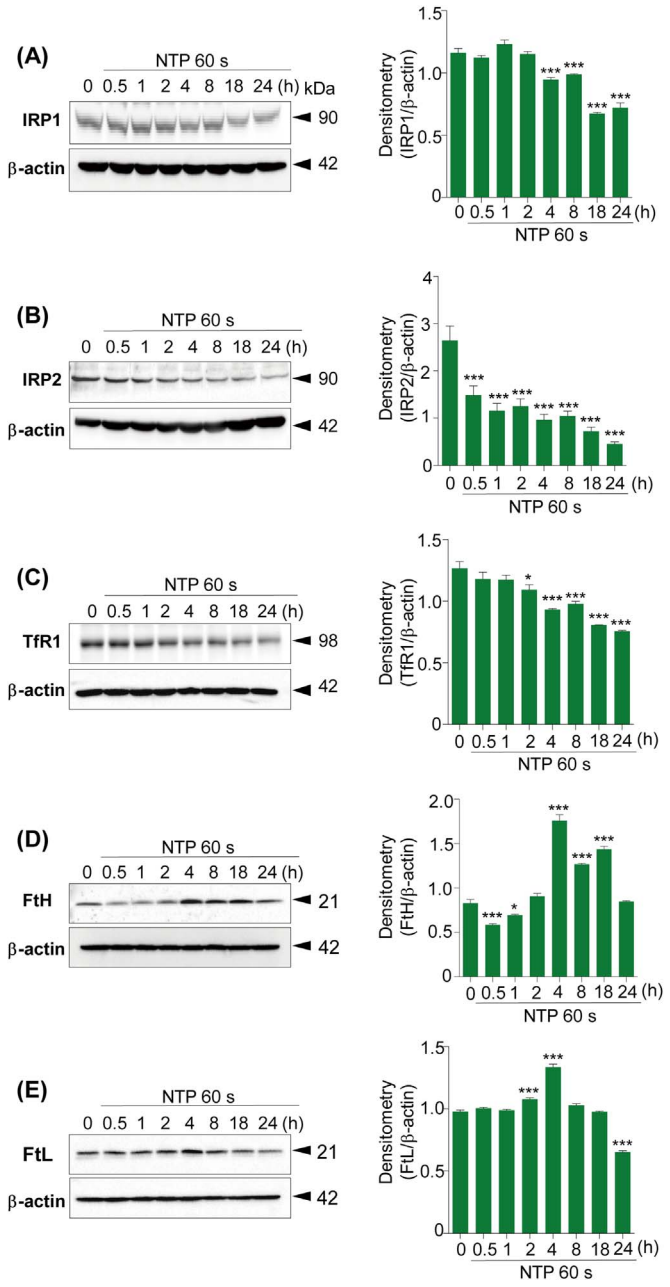

Fig. 3. NTP induces decreased total IRP1, total IRP2 and TfR1 protein expression, while transiently increasing FtH- and FtL-chain protein levels in SM2 malignant mesothelioma cells. The cells were treated with NTP (60 s) and then incubated in medium for either: 0, 0.5, 1, 2, 4, 8, 18, or 24 h/37 °C. The cells were then collected, and the expression of: **(A)** IRP1, **(B)** IRP2, **(C)** TfR1, **(D)** FtH and **(E)** FtL was examined in NTP-treated SM2 cells using western blot analysis. Densitometry was utilized to quantify changes. The blots shown are from typical experiments of the 3 performed, while the densitometry is shown as the mean ± SEM ($n = 3$). *, $p < 0.05$; ***, $p < 0.001$ *vs.* control.

their ability to post-transcriptionally alter transferrin receptor 1 (TfR1) and ferritin expression [58,59].

In these studies, SM2 mesothelioma cells were treated for 60 s with NTP and then incubated in complete medium for 0.5–24 h/37 °C. Relative to the 0 h time point, the expression of both IRP1 and IRP2 proteins was significantly ($p < 0.001$) decreased after NTP exposure times of 4–24 h and 0.5–24 h, respectively (Fig. 3**A, B**). Furthermore, a significant ($p < 0.001$–0.05) decrease in TfR1 was observed from 2 to 24 h (Fig. 3**C**). Examining ferritin-H (FtH; Fig. 3**D**) and ferritin-L (FtL; Fig. 3**E**) expression, there was transient and significant ($p < 0.001$) increase between 4–18 h and 2–4 h, respectively. For both FtH and FtL, the increase in their levels was subsequently followed by a decrease in expression. In fact, FtH decreased after 24 h to the levels found at the 0 h time point (Fig. 3**D**), while there was a significant ($p < 0.001$) decrease in FtL after a 24 h incubation relative to the 0 h time point (Fig. 3**E**). For both FtH and FtL, the transient increase in expression followed by the decrease could be interpreted to suggest an initial cellular response to NTP treatment to store iron, which is then subsequently followed by a decrease in storage.

The decrease in TfR1 and the increase in FtH and FtL expression could be due, in part, to the decrease in IRP1 and -2 levels that occurred after NTP exposure at 0.5–24 h. Indeed, the significant alterations in TfR1, FtH and FtL expression occurred at approximately the same time (*i.e.*, from 2 to 4 h incubation), as the significant alterations in IRP1 and IRP2 levels, which were first observed at 4 and 0.5 h, respectively (Fig. 3**A, B**).

As a relevant control to the investigations above, to assess the immediate effects of NTP on protein expression, cells were exposed to NTP (60 s) followed by no incubation period (Supplementary Fig. S2). These studies demonstrated no significant ($p > 0.05$) alterations in protein expression and are in contrast to results shown in Fig. 3 and other subsequent studies (*i.e.*, Figs. 5**B, D,** 6**B, C**), where NTP is followed by incubations of 0.5–24 h/37 °C. These results demonstrate that the changes observed in protein expression are a cellular response requiring metabolic alteration and were not due to a direct effect of the ionizing activity of NTP.

Overall, the data in Fig. 3 suggest that NTP results in a biological effect that generally resembles the cellular response observed after iron-loading, namely, decreased total IRP1 and IRP2 levels, decreased TfR1 and increased FtH and FtL expression [58].

3.6. NTP decreases the binding of IRPs to the IRE mRNA probe

The western blot analysis above of IRPs, particularly the down-regulation of IRP2 and TfR1 and the transient up-regulation of FtH and FtL chains, suggested an increase in cellular iron content after NTP treatment. Both the regulation of TfR1 and FtH and FtL chains by iron is mediated through the well-described IRP-IRE mechanism [58,60]. As IRP-IRE-binding is reduced upon increased intracellular iron, studies assessed this using a well-characterized gel-shift assay [61,62] (Fig. 4**A**).

In these studies, SM2 cells were treated with NTP for 60 s and then incubated for 0–8 h. As SM2 cells are derived from rats, IRP1 and IRP2 migrate in native gels as separate entities, with IRP1 migrating above IRP2 [63,64]. As a positive control to increase IRP-IRE binding, SM2 cells were also incubated with DFO (100 μM) for 24 h/37 °C, as it is known to induce cellular iron-depletion and pronounced IRP-IRE-binding activity (Fig. 4**A**). Indeed, after treatment with DFO, IRP1-IRE-binding activity was marked, with very little IRP2-IRE-binding being evident. At the 0–8 h time point after NTP treatment, only the IRP1 band was detected (Fig. 4**A**), indicating that IRP2-IRE-binding was below the detection limit using this methodology. Clearly, this result was in contrast to the more sensitive western analysis, where IRP2 protein expression was readily detected (Fig. 3**B**).

The binding of IRP1 to the *IRE* mRNA probe was slightly decreased following NTP and a 2 h incubation and this became a significant ($p < 0.001$–0.05) decrease in IRP1-IRE binding after a 4- and 8-h incubation after NTP treatment (Fig. 4**A**). The decrease in IRP1-IRE binding is consistent with the reduction observed in total IRP1 protein levels between 4–24 h and the down-regulation of TfR1 and up-regulation of FtH and FtL levels measured by western blotting (Fig. 3**A, C-E**). Collectively, the studies in Figs. 3 and 4**A** suggest an increase in cellular iron levels after NTP treatment and the regulation of TfR1, FtH and FtL expression *via* the well-characterized IRP-IRE regulatory mechanism [58,60].

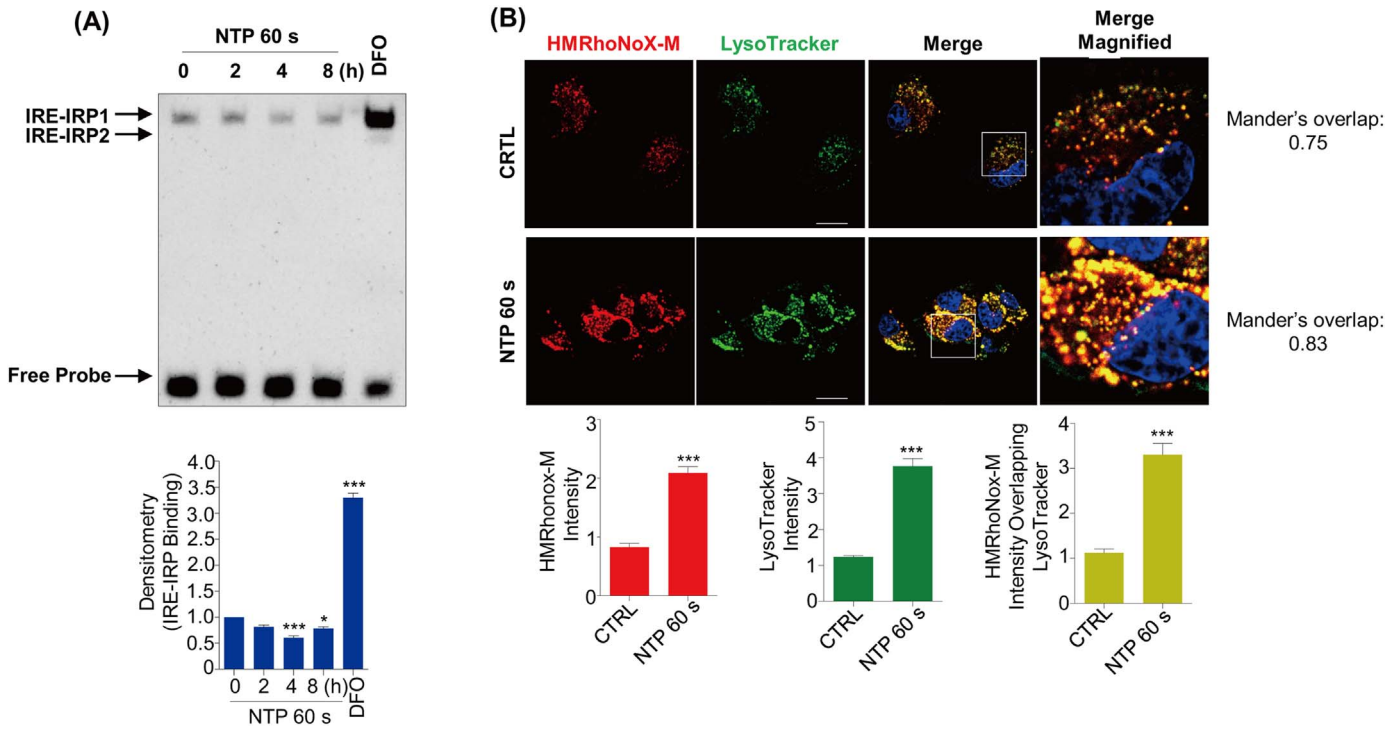

Fig. 4. NTP decreases the binding of IRP to *IRE* mRNA and promotes an increase in lysosomal ferrous iron in malignant mesothelioma SM2 cells. (A) SM2 cells were treated with NTP for 60 s and incubated for 0–8 h/37 °C. As a positive control, to induce increased IRP-IRE binding the cells were also incubated for 24 h with the specific iron chelator, desferrioxamine (DFO; 100 μM). A gel shift assay for *IRE* mRNA was performed using the Light Shift Chemiluminescent RNA EMSA Kit. **(B)** After treatment with NTP (60 s) and an incubation of 4 h/37 °C, the cells were stained for 30 min/37 °C with either LysoTracker Green DND-26 (green; 200 nM) or HMRhoNox-M (red; 10 μM). The yellow punctate staining demonstrates the electronic merge (Merge) of LysoTracker and HMRhoNox-M. The cells were examined using live cell imaging *via* confocal microscopy. The data are typical photographs from 3 experiments, with the data analysis shown as the mean ± SEM ($n = 3$). *, $p < 0.05$; ***, $p < 0.001$ *vs.* 0 h. Scale bar = 20 μm. (For interpretation of the references to color in this figure legend, the reader is referred to the web version of this article.)

3.7. NTP induces increased lysosomal iron levels

Considering the marked alterations in iron homeostasis proteins that indicated an increase in cellular iron levels after NTP (Figs. 3, 4**A**), studies were then designed to investigate cellular ferrous iron levels using the catalytic Fe(II)-specific probe HMRhoNox-M (red) [38] and its co-localization with the lysosomal-specific marker LysoTracker (green) [65]. These assays examining the co-localization of catalytic Fe(II) within lysosomes were performed as it is well known that the lysosome plays a key role in cellular iron metabolism, particularly with respect to the catabolism of ferritin and the release of iron from this protein [66,67].

In these studies, SM2 cells were treated with or without NTP (60 s), followed by incubation in complete medium for 4 h/37 °C (Fig. 4**B**). Cells without NTP treatment demonstrated weak punctate staining after incubation with the HMRhoNox-M (red) and LysoTracker probes (green) that showed co-localization in the merge (yellow), having a Mander's co-localization coefficient of 0.75 (Fig. 4**B**). These observations suggested that under basal conditions, lysosomes contained low quantities of catalytic iron, which is in good agreement with the known role of the lysosome in degrading ferritin and other iron-containing proteins *via* autophagy [66,67].

Interestingly, there was a marked and significant ($p < 0.001$) increase in the intensity of the punctate HMRhoNox-M and LysoTracker staining after NTP treatment (Fig. 4**B**). This increase in the intensity of staining from both probes was accompanied by a significant ($p < 0.001$) increase in their co-localization, as indicated by the Mander's co-localization coefficient increasing from 0.75 to 0.83 (Fig. 4**B**). The increase in Lysotracker staining suggested an increase in the number of lysosomes after NTP exposure, which is known to occur after exposure to other stress stimuli [68]. Further, the increase in catalytic iron detected by HMRhoNox-M is consistent with the induction of the catabolic autophagic process, with the liberation of iron from iron-containing proteins such as ferritin, *etc*.

3.8. NTP increases cellular lysosomal content via endocytosis/pinocytosis

The lysosome number per cell and lysosomal iron levels were increased after treatment with NTP (Fig. 4**B**), suggesting a potential increase in autophagy, which is involved in cellular iron turnover *via* the lysosome [69]. Recently, it has been shown that cellular stress stimuli can result in increased endocytosis and lysosome formation [68,70,71]. Thus, it was hypothesized that this process may be responsible for the increased autophagy after NTP. To examine this hypothesis, confocal microscopy was used to examine the immunofluorescent staining of the early endosome marker, early endosomal antigen 1 (EEA1), and the uptake of pHrodo Red Dextran, which is a marker of non-specific, fluid-phase endocytosis [70] (Fig. 5**A**).

Treatment of SM2 cells with NTP (60 s) followed by an incubation for 4 or 8 h caused a significant ($p < 0.001$) time-dependent increase in pHrodo Red Dextran uptake (red) after 4 h or 8 h relative to the 0 h control. In contrast, EEA1 (green) staining increased significantly ($p < 0.05$) after 4 h relative to the 0 h control and then decreased to near control levels at 8 h (Fig. 5**A**). Limited co-localization (yellow) in the merge was only observed after 2, 4 and 8 h of incubation, with the Mander's co-localization coefficient at these time points being 0.18, 0.32 and 0.40, respectively (Fig. 5**A**). Similarly, western analysis also suggested a slight, but significant ($p < 0.001$–0.05) increase in EEA1 expression after exposure to NTP at 4, 18 and 24 h of incubation (Fig. 5**B**). Together, these results suggested that NTP resulted in a progressive time-dependent increase in non-specific fluid-phase pinocytosis (as judged by pHrodo Red Dextran uptake) leading to EEA1-stained endosomes, as observed for other stress stimuli [68].

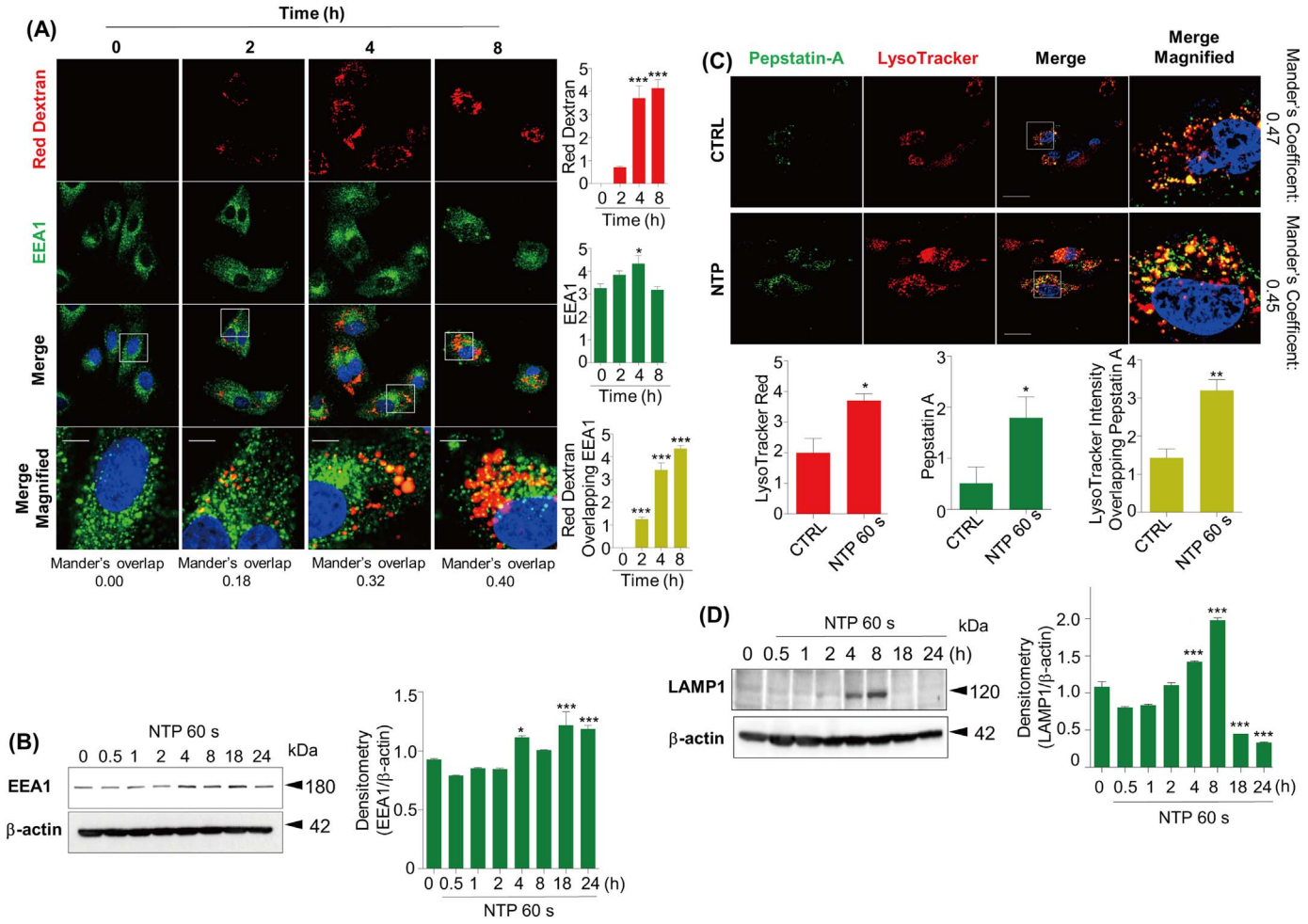

Fig. 5. NTP increases pHrodo Red Dextran uptake by cells suggesting stimulation of fluid-phase endocytosis and it also induces endosome and lysosome formation in malignant mesothelioma SM2 cells. (A) Cells were treated with NTP (60 s) and then incubated for 0, 2, 4 or 8 h/37 °C with pHrodo Red Dextran (10 μg/mL) and EEA1 antibody (1/1000 dilution). The cells were then examined using confocal microscopy, and nuclear counterstaining was performed using DAPI. **(B)** SM2 cells were treated with or without NTP (60 s) and then incubated for 0.5, 1, 2, 4, 8, 18 or 24 h/37 °C. The cells were collected, and the expression of EEA1 (1:1000) was assessed by western blot analysis. **(C)** SM2 cells were treated with or without NTP (60 s) and then incubated for 4 h/37 °C. The cells were then incubated for an additional 30 min/37 °C with the lysosomal markers, LysoTracker Red (200 nM) and Pepstatin A-BODIPY FL conjugate (1 μM). The electronic merge (Merge; yellow) between LysoTracker Red (red fluorescence) and Pepstatin A-BODIPY FL (green fluorescence) is shown. The cells were observed using live cell imaging *via* confocal microscopy. **(D)** SM2 cells were treated under the same conditions as (B), and the expression of LAMP1 (1:500) was assessed by western blot analysis. The data are typical of 3 experiments, and the analysis/densitometry is shown as the mean ± SEM ($n = 3$). *, $p < 0.05$; **, $p < 0.01$; ***, $p < 0.001$ *vs.* control. Scale bar = 20 μm. (For interpretation of the references to color in this figure legend, the reader is referred to the web version of this article.)

To further examine the hypothesis that NTP acted as a cellular stress to increase lysosome formation, our studies then assessed the co-localization of the well-characterized lysosomal markers, Pepstatin A Bodipy FL conjugate (green) and LysoTracker (red; Fig. 5**C**). Under control conditions, both markers in SM2 cells resulted in weak punctate staining with some co-localization being evident in the merge (yellow; Mander's co-localization coefficient: 0.47), suggesting low lysosomal content. After treatment of SM2 cells with NTP (60 s) and an incubation of 4 h, there was a marked and significant ($p < 0.05$) increase in the staining of both lysosomal markers resulting in yellow fluorescence, which is indicative of co-localization in the merge (Mander's co-localization coefficient: 0.45) (Fig. 5**C**).

Furthermore, as another indicator of lysosome formation after NTP, western analysis was performed to assess the well characterized lysosomal marker, LAMP1 [72]. This was examined by exposing SM2 cells to NTP for 60 s and then incubating these cells for 0.5–24 h/37 °C (Fig. 5**D**). Relative to the 0 h time point, there was a significant ($p < 0.001$) increase in LAMP1 expression after 4 and 8 h relative to the 0 h time point. This increase was followed by a significant ($p < 0.001$) decrease in LAMP1 levels after 18 and 24 h of incubation (Fig. 5**D**). These results can be speculated to suggest the induction of lysosomal biogenesis for autophagy by NTP followed by the catabolism of LAMP1 during this catabolic process. Such kinetics of LAMP1 expression during the induction of autophagy have been demonstrated under other experimental conditions [73]. In summary, these results in Figs. 4 and 5 demonstrate that NTP increases cellular lysosomal content and may result in the induction of autophagy.

3.9. NTP induces autophagy in mesothelioma cells

The results above in Figs. 4**B,** 5**C,** and **D** demonstrate that NTP induces a marked increase in lysosomes, which are known to be involved in autophagy [73,74]. To directly assess the induction of autophagy, LC3B, a classical marker of the autophagosome that directly correlates with autophagosome number [75] was examined.

In initial studies, SM2 mesothelioma cells were treated for 60 s with NTP or the control and then incubated with complete medium for 0–8 h, and the presence of LC3-containing autophagosomes was assessed by confocal microscopy (Fig. 6**A**). Relative to the 0 h time point, NTP induced a pronounced and significant ($p < 0.001$) increase in LC3B fluorescence (red) intensity, which peaked after a 2-h incubation and then decreased up to 8 h (Fig. 6**A**). In contrast, treatment of

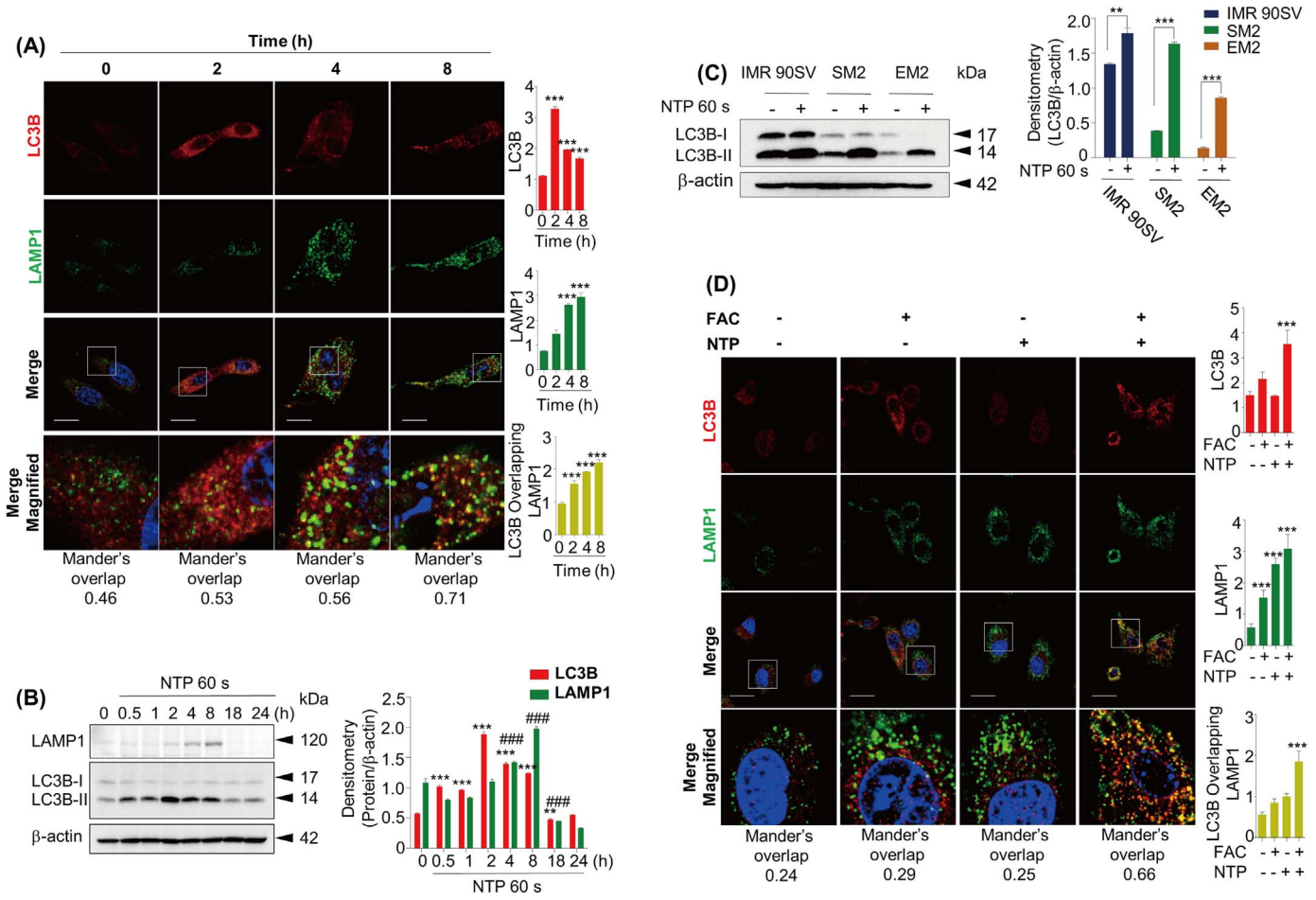

Fig. 6. NTP-induced autophagy is observed in malignant mesothelioma SM2 cells and is potentiated by incubation with iron as ferric ammonium citrate (FAC). (A) The cells were treated with NTP (60 s), and after an incubation of 0, 2, 4 or 8 h/37 °C, they were fixed with 4% paraformaldehyde at room temperature. After blocking, SM2 cells were then incubated with anti-LAMP1 (1:500) and anti-LC3B (1:1000) antibodies overnight at 4 °C. The cells were observed using confocal microscopy. Scale bar = 20 μm. **(B)** SM2 cells were treated with or without NTP (60 s) and then incubated for 0.5, 1, 2, 4, 8, 18 or 24 h/37 °C. The cells were collected, and the expression of LAMP1 and LC3B-I and -II was assessed by western blot analysis. β-actin was used as a loading control. * indicates the significance value for LC3B, while # indicates the significance for LAMP1. **, $p < 0.01$; ***, $p < 0.001$ *vs.* control. ###, $p < 0.001$ *vs.* control. **(C)** IMR 90SV fibroblasts, SM2 cells and EM2 cells were treated with NTP (60 s) and then incubated for 2 h/37 °C. The cells were collected, and the expression of LAMP1 and LC3 was assessed by western blot analysis. β-actin was used as a loading control. **(D)** SM2 cells were pre-incubated with or without FAC (6.6 μg/mL) for 3 h/37 °C and then treated with NTP (30 s). The cells were then incubated for a further 4 h/37 °C, fixed and stained with anti-LAMP1 and anti-LC3B antibodies. These data are typical photographs from 3 experiments with the analysis/densitometry shown as the mean ± SEM ($n = 3$). Scale bar = 20 μm.

SM2 cells with NTP resulted in a significant ($p < 0.001$) time-dependent increase in LAMP1 levels (green) at 4 h and 8 h of incubation (Fig. 6**A**). Examination of the co-localization of LAMP1 and LC3B indicated a significant ($p < 0.001$) increase in yellow fluorescence in the merge, which demonstrated a time-dependent increase up to 8 h and a corresponding increase in the Mander's co-localization coefficient from 0.46 at 0 h, to 0.71 after an 8-h incubation (Fig. 6**A**). The increase in LC3B suggested the presence of autophagosomes [76], while the co-localization of LC3 and the LAMP1 lysosomal marker suggested autophagolysosome formation [77]. Notably, the fluorescent vesicles which may comprise autophagolysosomes (yellow overlay fluorescence) as well as other LAMP1 positive constituents of the lysosomal compartment, show a considerable size increase between 0 and 8 h (Fig. 6**A**). The reason for this observation may be the maturation of these vesicles into active digestive organelles.

To quantitatively evaluate lysosome and autophagolysosome formation, immunoblotting was performed to determine the LAMP1 and LC3B levels after a 60-s treatment of SM2 cells with NTP followed by 0–24 h incubation in complete medium (Fig. 6**B**). In these studies, and in agreement with the analysis from confocal microscopy (Fig. 6**A**), and the western analysis in Fig. 5**D**, the LAMP1 band was significantly ($p < 0.001$) increased after 4 and 8 h relative to the 0 h control and then decreased (Fig. 6**B**). On the other hand, two LC3B bands were found at 17 and 14 kDa at all time points, which are well known to correspond to LC3B-I and LC3B-II, respectively [75] (Fig. 6**B**). The conversion of LC3B-I to LC3B-II *via* lipidation is critical for autophagosome formation, and hence, a low level of autophagy was demonstrated in the control cells, as expected [78]. Upon a 60-s treatment with NTP, the levels of LC3B-I expression were not significantly ($p > 0.05$) altered at all incubation times relative to the 0-h control (Fig. 6**B**). In contrast, a marked and significant ($p < 0.001$) increase in the LC3B-II level relative to the control was evident after a 0.5 h incubation and peaked at 2 h and then decreased (Fig. 6**B**). This observation was in good agreement with the confocal microscopy analysis in Fig. 6**A**.

As additional evidence for the induction of autophagy in SM2 cells after exposure to NTP, the expression and subcellular localization of the transcription factor EB (TFEB) was examined, which is known to be pivotal for lysosomal biogenesis and autophagy [79]. As entrance into the nucleus is required for TFEB transcriptional activity [80], its expression in nuclear and cytoplasmic fractions were assessed as a function of time (0–24 h) after a 60 s exposure to NTP (Supplementary Fig. S3). In these studies, nuclear TFEB levels were rapidly and significantly ($p < 0.001$) increased 0.5 h after the NTP dose and peaked after 1 h to levels > 3.5-fold that found at 0 h. After 1 h, nuclear TFEB

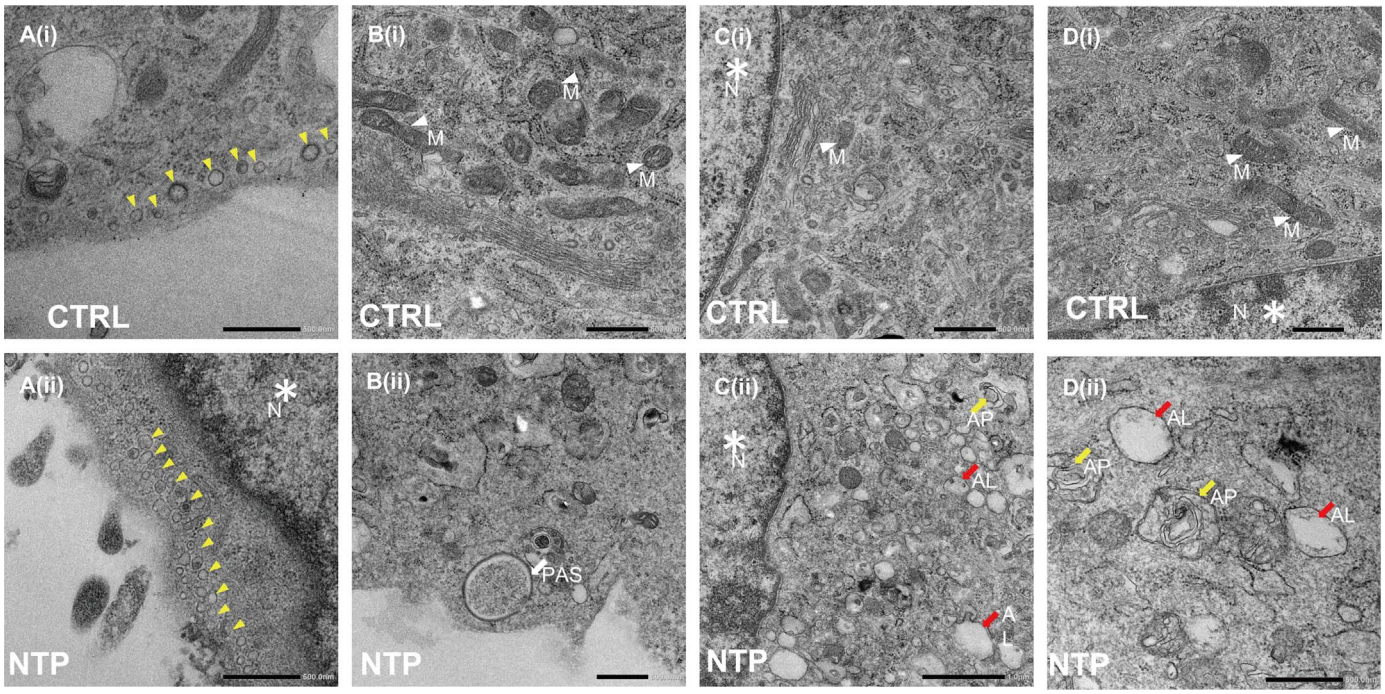

Fig. 7. Transmission electron micrographs demonstrating vesicle structures consistent with endosome-like vesicles and organelles of the autophagic pathway. Electron micrographs showing the ultrastructure of SM2 cells treated with or without NTP (60 s) and then incubated for 4 h/37 °C. **Ai, Bi, Ci, Di** Control (CTRL) micrographs. Yellow arrowheads indicate endosome-like vesicles. White arrowheads indicate mitochondria (M). The nucleus (N) is indicated by an asterisk. **Aii, Bii, Cii, Dii** NTP-treated micrographs. Yellow arrowheads indicate endosome-like vesicles. Pre-autophagic structures (PAS), autophagosomes (AP), or autophagolysosomes (AL) are shown by white or red arrows. The nucleus (N) is indicated by an asterisk. Scale Bar **Ai, Bi, Ci, Di:** 0.5 μm; **Aii, Bii, Dii** 0.5 μm; **Cii** 1 μm. The results are typical micrographs from 3 different experiments. (For interpretation of the references to color in this figure legend, the reader is referred to the web version of this article.)

expression then gradually decreased as a function of time up until 18 h, where its levels were similar to that at 0 h (Supplementary Fig. S3). The increase in nuclear TFEB was accompanied by a general decrease in cytoplasmic TFEB at time points 0.5–18 h after the exposure to NTP. Thus, in summary, these results were consistent with the translocation of TFEB from the cytosol into the nucleus.

The effect of NTP treatment on the conversion of LC3-I–LC3-II was then assessed using IMR 90SV fibroblasts relative to SM2 and EM2 mesothelioma cells after a 4 h incubation (Fig. 6**C**). Both LC3B-I and LC3B-II expression were markedly and significantly ($p < 0.001$) higher in untreated IMR 90SV fibroblasts than in untreated SM2 and EM2 mesothelioma cells. There was a slight, but significant ($p < 0.01$) increase in LC3B-I and II upon NTP treatment of fibroblasts (Fig. 6**C**). In contrast, using SM2 and EM2 cells, treatment with NTP induced a marked and significant ($p < 0.001$) increase in LC3B-II expression relative to untreated control cells (Fig. 6**C**). These data suggested that LC3B-II autophagic marker demonstrated a more robust increase in the tumorigenic mesothelioma cells relative to the non-tumorigenic fibroblasts. This response correlates to the increased susceptibility of both SM2 and EM2 cells to NTP relative to the non-tumorigenic IMR 90SV fibroblasts (Fig. 1**Aii**).

In summary, NTP markedly induced: **(i)** LC3B-II, suggesting autophagosome formation; **(ii)** the rapid nuclear translocation of TFEB that is important for lysosomal biogenesis and autophagy; and **(iii)** the generation of autophagolysosomes, as demonstrated by the co-staining of LAMP1 and LC3B.

3.10. NTP increases LAMP1 and LC3B to a greater extent after incubation with FAC

Since NTP increased lysosomal content (Fig. 5**C, D;** Fig. 6**A, B**), and as FAC was shown to increase the efficacy of NTP in terms of decreasing cell viability (Fig. 1**Ci**), studies were then performed using confocal microscopy to assess the effect of FAC on LAMP1 and LC3B expression (Fig. 6**D**). In these experiments, SM2 mesothelioma cells were pre-incubated with complete medium with or without FAC (6.6 μg/mL) for 3 h/37 °C, treated for 30 s with NTP and then incubated for a further 4 h/37 °C. Confocal microscopy was then performed to detect LAMP1 and LC3B expression.

Interestingly, incubation with FAC alone resulted in a slight increase in LC3B-I/II and a significant ($p < 0.001$) increase in punctate LAMP1 staining relative to cells incubated with medium alone (Fig. 6**D**). Treatment with NTP itself (30 s) followed by a 4-h incubation, resulted in no change in LC3B expression (Fig. 6**D**). Furthermore, NTP alone led to an increase in LAMP1 expression that was significantly ($p < 0.001$) greater than that of the untreated control (Fig. 6**D**), and this was in good agreement with the western analysis examining LAMP1 levels (Fig. 6**B**). The combination of NTP treatment and incubation with FAC resulted in the most marked and significant ($p < 0.001$) increase in LC3B and LAMP1 expression, which was greater than all other conditions (Fig. 6**D**). Moreover, the co-localization of LAMP1 and LC3B in the overlap (yellow) was only significant ($p < 0.001$) for the FAC and NTP combination relative to the control without FAC and NTP. In fact, after treatment with FAC and NTP, the Mander's overlap coefficient was 0.66, which was markedly increased relative to the value observed for either the control without FAC or NTP (0.24), FAC (0.29) or NTP alone (0.25; Fig. 6**D**). These studies suggest that FAC potentiates the effects of NTP in inducing LC3B and LAMP1 expression, probably due to an iron-dependent increase in cellular ROS levels.

3.11. Electron microscopic identification of structures consistent with increased endocytosis and autophagic vacuoles after NTP

The results above strongly suggest that NTP induces fluid-phase endocytosis in SM2 cells (Fig. 5**A**), increased early endosome levels (Fig. 5**A, B**), lysosome formation (Fig. 5**C, D**), and autophagy (Fig. 6). Hence, to further validate these changes, we performed transmission electron microscopy to assess the presence of endosomes, lysosomes

and autophagic vacuoles in SM2 cells after NTP (60 s) and a 4 h/37 °C incubation relative to the control cells (Fig. 7). These studies confirmed the results obtained with confocal microscopy above and demonstrated the presence of structures that were morphologically consistent with increased endosomes and autophagic organelles after NTP relative to mitochondria (M) and the nucleus (N; indicated by asterisk; Fig. 7).

Relative to the CTRL (Fig. 7**Ai**), and close to the plasma membrane in the NTP-treated cells (Fig. 7**Aii**), there was a pronounced increase in small vesicles consistent with endosomes with sizes up to ~60 nm in diameter. This observation is in good agreement with the effect of NTP on increasing pHrodo Red Dextran uptake by cells *via* fluid-phase endocytosis (Fig. 5**A**) and EEA1 expression (Fig. 5**B**), which is a classical marker of early endosomes [81]. These results also concur with previous studies using other stress stimuli, where increased fluid-phase endocytosis, early endosome formation and elevated lysosome levels were reported [68].

In addition, in CTRL SM2 cells, very few autophagic vacuoles were apparent (Fig. 7**Ai–Di**), again in good agreement with studies assessing LC3B expression (Fig. 6; indicative of autophagosomes; [73,82]) and also LC3B col-localization with LAMP1 (Fig. 6**A;** indicative of autophagolysosomes [83]). However, upon treatment with NTP (60 s) followed by a 4-h incubation in complete medium, there was a marked alteration in cellular morphology with a pronounced increase in autophagic vacuoles being obvious (Fig. 7**Bii–Dii**). These vacuoles were up to ~500 nm in size and had morphological characteristics typical of various stages of organelles in the autophagic progression pathway [84]. For example, in Fig. 7**Bii, Cii,** and **Dii**, organelles consistent with the morphology of the pre-autophagic structure (*i.e.,* phagophore; PAS), autophagosome (AP) and late-stage autophagolysosome (AL) [84] were observed. These data are consistent with the results from Fig. 6**A** demonstrating the co-localization of LC3B and LAMP1 and Fig. 6**B** demonstrating the marked increase in LC3B-II, which are classical markers of the autophagolysosome and autophagosome, respectively, and indicate autophagic induction [85,86].

In summary, NTP induces a cellular stress response probably mediated through ROS generation (Fig. 2), which results in a marked increase in fluid-phase endocytosis/pinocytosis, early endosome formation, lysosome biogenesis and autophagy **(**Figs. 6–8**).**

4. Discussion

For the first time, NTP was demonstrated to induce a stress response in malignant mesothelioma cells that constituted increased oxidative stress, endocytosis, lysosome formation, and autophagy. This effect was important to characterize in terms of understanding the anti-proliferative activity and efficacy of NTP against neoplastic mesothelioma cells. While previous studies have assessed the effect of NTP on many tumor cell-types in culture, these studies have been confined to assessing alterations in proliferation, cell cycle arrest and DNA damage [87–89]. At present, due to resistance mechanisms, new regimens of cancer treatment are crucial to explore, and NTP represents a new therapeutic strategy. However, the mechanisms responsible for the anti-tumor efficacy of this form of ionizing radiation remain largely unknown and were the subject of this investigation.

An important observation in the current study was the selective anti-proliferative activity of NTP against malignant mesothelioma cells relative to non-tumorigenic fibroblast cell lines. This finding was in contrast to the general lack of selectivity observed with the chemotherapeutic, cisplatin, which is used for the treatment of malignant mesothelioma. This selectivity indicates that NTP has potential anti-tumor activity that could be related to the differences observed in ROS generation between the normal and tumor cells in 3 different assays. This difference in the production of ROS could be related to a variety of differences between normal and neoplastic cells, including: **(i)** iron content; **(ii)** anti-oxidative systems; **(iii)** autophagic processing; and **(iv)** rates of proliferation [90].

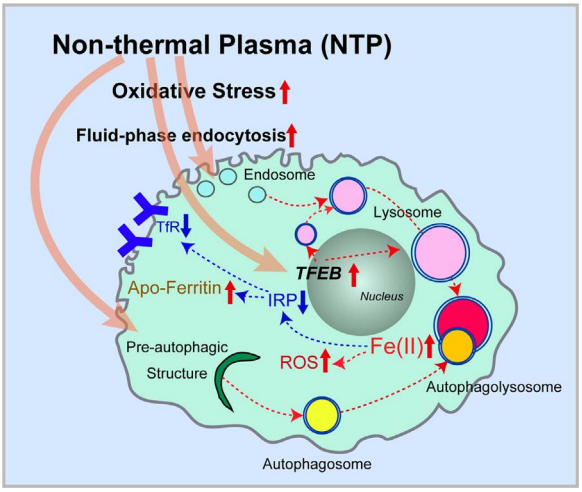

Fig. 8. Schematic demonstrating the response of malignant mesothelioma cells to NTP with the production of ROS that is induced through the reaction with cellular iron. This acts as a stress stimulus that leads to increased fluid-phase endocytosis, lysosomal biogenesis and autophagy. The induction of ROS by NTP (demonstrated by the CM-H2DCFDA, MitoSOX, and C11-BODIPY probes) results in cellular stress that leads to increased fluid-phase endocytosis (demonstrated by pHrodo Red Dextran uptake) and the increased formation of endosomes and lysosomes (shown *via* western blot analysis as well as confocal and electron microscopy). Treatment of cells with NTP results in a marked and rapid nuclear translocation of the transcription factor, TFEB, which is a master regulator of lysosomal biogenesis and autophagy. The initiation of autophagy promotes the removal of damaged cellular constituents after NTP-induced ROS generation and the liberation of iron from iron-containing proteins (demonstrated by co-localization of catalytic Fe(II)-selective probe, HMRhoNox-M, and Lysotracker) that can be used for repair, or stored in ferritin.

Each of these latter factors has been demonstrated to be distinctly different between normal and neoplastic cells. For example, first, neoplastic cells are known to commonly internalize iron from transferrin at higher rates due to marked expression of the transferrin receptor 1 [91,92]. Second, tumor cells generally express lower levels of anti-oxidant enzymes, such as glutathione peroxidase, catalase and superoxide dismutase relative to normal cells [93], and thus, are oxidatively-stressed [94]. Third, autophagic processing is known to be increased in most contexts in cancer cells to facilitate oncogenesis, tumor growth and survival [95]. Finally, cancer cell growth is generally more rapid *in vivo* than that of normal cells, which could lead to susceptibility to NTP due to alterations in iron metabolism that cause increased levels of cellular iron that can result in enhanced ROS [96].

Considering this latter factor, a critical finding in this investigation was the novel demonstration that cellular iron-loading with FAC could potentiate the efficacy of NTP. Moreover, the effect of NTP could also be potently inhibited by cellular iron chelation using DFO, which is known to deplete iron pools [97]. The effect of iron in facilitating NTP activity is probably related to its ability to generate intracellular ROS that facilitates the iron-catalyzed Fenton/Haber-Weiss reaction, which potentiates oxidative stress through increased cytotoxic radical generation [98]. Interestingly, the effect of iron on potentiating NTP activity is similar to the enhanced activity of ionizing radiation (*i.e.*, photon beam) observed in iron-loaded prostate cancer cells [99]. Again, this may be due to the ability of iron to potentiate ROS generation *via* Fenton/Haber-Weiss chemistry [47,100,101].

Regarding the potentiating interaction of iron in terms of NTP efficacy, studies were designed to assess the expression of proteins involved in the metabolism of this metal ion after treatment of cells with NTP. A transient increase in the expression of the FtH and FtL and decrease in TfR1 levels were observed after NTP treatment of malignant mesothelioma cells (Fig. 3**C, D**). This response may indicate increased levels of cellular labile iron [102–104]. In fact, it is well known that elevated cellular iron levels increase ferritin and decrease TfR1 by a

mechanism that involves the sensing of iron by IRP1 and IRP2 [58]. A notable response in this study was the marked down-regulation of both IRP1 and IRP2 protein levels after NTP treatment, which could potentially be responsible for the effects on ferritin and TfR1 expression. At the same time, the decreased binding of IRP1 to the IRE as judged by the gel-retardation assay again confirmed that cytoplasmic iron was significantly increased after NTP treatment.

Of interest, NTP increased FtH to a greater extent than FtL, and this may be related to the role of FtH in oxidizing Fe(II) to catalytically inactive Fe(III) within ferritin, which is protective, as demonstrated under other conditions [105]. This would result in decreased levels of cellular iron that have been shown here to facilitate anti-proliferative activity of NTP in malignant mesothelioma cells (Fig. 1**Ci**). Evidence of a transient increase in cellular iron that could up-regulate ferritin-H and down-regulate TfR1 was indicated in our studies using the specific Fe (II) probe HMRhoNox-M, which demonstrated increased co-localization with the LysoTracker probe after NTP exposure. This observation was consistent with increased cellular levels of lysosomes (Figs. 4**B and** 6**B, C**) and substantial evidence that NTP resulted in autophagy (Figs. 6**A–D**, 7**Bii–Dii**; Suppl. Fig. S3). These data included the rapid nuclear translocation of TFEB that is a major regulator of lysosomal biogenesis and autophagy [106,107] **(**Fig. S3**).** The marked up-regulation of TFEB in the nucleus occurred 0.5 h after NTP exposure and was observed concurrently with the increase in LC3B. Collectively, these studies indicate a mechanism by which NTP induces autophagy (Fig. 8) *via* ROS generation (Fig. 2**Ai–iii**), increased fluid-phase endocytosis (Fig. 5**A**), an increase of early endosomes (Fig. 5**A, B**) and lysosomes (Fig. 5**C, D**), and the induction of autophagic vesicles (Fig. 7).

Such a response to NTP involving autophagy could be induced as a protective repair mechanism that leads to the cellular turnover of proteins and organelles that include iron-containing constituents, leading to the liberation of the metal in lysosomes (as observed in Fig. 4**B**). Hence, the lysosomes that accumulate in NTP-treated cells are functional in terms of degradative capacity. A similar cellular response has been reported in cells incubated under other stress stimuli, *e.g.,* hypo- and hyper-glycemic conditions, in which ROS generation was shown to induce fluid-phase endocytosis and increase lysosome formation [68,108]. However, this is the first report demonstrating that NTP also acts *via* this mechanism. In fact, we propose a link between stress-triggered endo-/pinocytosis (heterophagy) and the pronounced autophagy observed after NTP treatment. Nonetheless, the fusion of autophagosomes with lysosomes, which are not derived from an endo-/pinocytosis process *e.g.*, de-novo synthesized lysosomes, could also substantially contribute to the enhanced autophagy observed. Considering this, it is notable that TFEB is markedly increased after NTP that is involved in lysosomal biogenesis and autophagy (Supplemental Fig. S3) and autophagy is known to be induced by ROS through the regulation of the activity of autophagy-related 4 (ATG4) [109]. The ROS generated *via* NTP (Fig. 2) could be responsible for inducing this latter effect.

In terms of a comparison of the effects of NTP to other therapeutic modalities, it is of interest that ionization radiation has been reported to act somewhat similarly to NTP, leading to increased ROS generation [110] and the induction of autophagy [111]. In fact, autophagy has been reported to result in the catabolism of damaged cellular constituents and represents a key repair mechanism. Recently, it was reported that hepatoma cells may protect themselves from iron-dependent oxidative stress during lysosomal membrane permeabilization and the subsequent cytotoxicity by increasing the lysosomal content of metallothionein [112]. Such a response may be related to the observations in the current investigation. However, metallothioneins are generally known to be involved in the sequestration of other metal ions, such as zinc and copper, and thus, it may represent another protective mechanism against oxidative stress.

In summary, this investigation has demonstrated for the first time that NTP markedly increases cellular ROS levels with the generation of these species being dependent on intracellular iron. Hence, through this mechanism, NTP acts as a stress stimulus and results in an increase in endocytosis, early endosome and lysosome biogenesis, and the induction of autophagy (Fig. 8). Interestingly, NTP treatment led to a decrease in TfR1 expression and a transient increase in FtH- and FtL-chain, suggesting an increase in cellular iron levels. This latter effect after NTP probably was caused by the rapid induction of autophagy that is a catabolic response, which can induce the liberation of iron from cellular constituents (Fig. 8). Hence, it can be suggested that these observations represent an initial repair response to the stress induced by NTP-generated ROS. These results are important for understanding the mechanism of NTP action, as it is a burgeoning therapeutic option for the treatment of cancer.

Acknowledgments

This work was supported, in part, by the National Cancer Center Research and Development Fund (26-A-8), and JSPS KAKENHI Grant nos. JP24390094, JP16K15257, JP24108008 and JP17H04064 to S.T. Electron microscopic analyses were supported by Koji Itakura, Division of Medical Research Engineering, Nagoya University Graduate School of Medicine. D.R.R. thanks the National Health and Medical Research Council of Australia (NHMRC) for a Senior Principal Research Fellowship and Project Grants. D.R.R. also very much appreciates the award of a Japan Society for the Promotion of Science (JSPS) Invitation Fellowship that enabled this collaboration. Finally, Dr. Patric Jansson, Dr. Danuta Kalinowski, Dr. Zaklina Kovacevic and Dr. Darius Lane are kindly thanked for their helpful comments on manuscript prior to submission.

Appendix A. Supplementary information

Supplementary data associated with this article can be found in the online version at http://dx.doi.org/10.1016/j.freeradbiomed.2017.04.368.

References

[1] IARC, WHO, Asbestos (chrysotile, amosite, crocidolite, tremolite, actinolite, and anthophyllite), IARC Monographs on the Evaluation of Carcinogenic Risks to Humans, A Review of Human Carcinogens; Part C: Arsenic, Metals, Fibres, and Dusts, Lyon, France, 2012, pp. 219–309.
[2] A. Reid, N.H. de Klerk, C. Magnani, D. Ferrante, G. Berry, A.W. Musk, E. Merler, Mesothelioma risk after 40 years since first exposure to asbestos: a pooled analysis, Thorax 69 (2014) 843–850.
[3] J. Ribak, I.J. Selikoff, Survival of asbestos insulation workers with mesothelioma, Br. J. Ind. Med. 49 (1992) 732–735.
[4] F. Vlastos, G. Kaltsakas, J.-M. Vignaud, N.M. Martinet, N.G. Koulouris, Survival of mesothelioma patients after radical extrapleural pneumonectomy in the Nancy Biobank's database, Eur. Respir. J. 42 (Suppl. 57) (2013) SP3074.
[5] M. Dusinska, A. Collins, A. Kazimirova, M. Barancokova, V. Harrington, K. Volkovova, M. Staruchova, A. Horska, L. Wsolova, A. Kocan, J. Petrik, M. Machata, B. Ratcliffe, S. Kyrtopoulos, Genotoxic effects of asbestos in humans, Mutat. Res. 553 (2004) 91–102.
[6] S. Toyokuni, Mechanisms of asbestos-induced carcinogenesis, Nagoya J. Med. Sci. 71 (2009) 1–10.
[7] S.H. Chew, S. Toyokuni, Malignant mesothelioma as an oxidative stress-induced cancer: an update, Free Radic. Biol. Med. 86 (2015) 166–178.
[8] J.M.G. Davis, R.E. Bolton, J. Garrett, Penetration of cells by asbestos fibers, Environ. Health Perspect. 9 (1974) 255–260.
[9] L. Jiang, H. Nagai, H. Ohara, S. Hara, M. Tachibana, S. Hirano, Y. Shinohara, N. Kohyama, S. Akatsuka, S. Toyokuni, Characteristics and modifying factors of asbestos-induced oxidative DNA damage, Cancer Sci. 99 (2008) 2142–2151.
[10] R.A. Pietrofesa, A. Velalopoulou, S.M. Albelda, M. Christofidou-Solomidou, Asbestos induces oxidative stress and activation of Nrf2 signaling in murine macrophages: chemopreventive role of the synthetic lignan secoisolariciresinol diglucoside (LGM2605), Int. J. Mol. Sci. 17 (2016) 322.
[11] H. Nagai, T. Ishihara, W.H. Lee, H. Ohara, Y. Okazaki, K. Okawa, S. Toyokuni, Asbestos surface provides a niche for oxidative modification, Cancer Sci. 102 (2011) 2118–2125.
[12] Y. Kubo, H. Takenaka, H. Nagai, S. Toyokuni, Distinct affinity of nuclear proteins to the surface of chrysotile and crocidolite, J. Clin. Biochem. Nutr. 51 (2012) 221–226.
[13] S. Toyokuni, Oxidative stress as an iceberg in carcinogenesis and cancer biology, Arch. Biochem. Biophys. 595 (2016) 46–49.

[14] L. Jiang, S. Akatsuka, H. Nagai, S.H. Chew, H. Ohara, Y. Okazaki, Y. Yamashita, Y. Yoshikawa, H. Yasui, K. Ikuta, Iron overload signature in chrysotile-induced malignant mesothelioma, J. Pathol. 228 (2012) 366–377.
[15] D.E. Kamp, V.A. Israbian, S.E. Preusen, C.X. Zhang, S.A. Weitzman, Asbestos causes DNA strand breaks in cultured pulmonary epithelial cells: role of iron-catalyzed free radicals, Am. J. Physiol. 268 (1995) 471–480.
[16] J.K. Thompson, C.M. Westbom, M.B. MacPherson, B.T. Mossman, N.H. Heintz, P. Spiess, A. Shukla, Asbestos modulates thioredoxin-thioredoxin interacting protein interaction to regulate inflammasome activation, Part. Fibre Toxicol. 11 (2014) 1–13.
[17] W. Aung, S. Hasegawa, T. Furukawa, T. Saga, Potential role of ferritin heavy chain in oxidative stress and apoptosis in human mesothelial and mesothelioma cells: implications for asbestos-induced oncogenesis, Carcinogenesis 28 (2007) 2047–2052.
[18] H. Nagai, Y. Okazaki, S.H. Chew, N. Misawa, H. Yasui, S. Toyokuni, Deferasirox induces mesenchymal-epithelial transition in crocidolite-induced mesothelial carcinogenesis in rats, Cancer Prev. Res. 6 (2013) 1222–1230.
[19] M. Markman, S. Cleary, C. Pfeifle, S.B. Howell, Cisplatin administered by the intracavitary route as treatment for malignant mesothelioma, Cancer 58 (1986) 18–21.
[20] A. Rimner, M.G. Zauderer, D.R. Gomez, P.S. Adusumilli, P.K. Parhar, A.J. Wu, K.M. Woo, R. Shen, M.S. Ginsberg, E.D. Yorke, D.C. Rice, A.S. Tsao, K.E. Rosenzweig, V.W. Rusch, L.M. Krug, Phase II Study of hemithoracic intensity-modulated pleural radiation therapy (IMPRINT) as part of lung-sparing multi-modality therapy in patients with malignant pleural mesothelioma, J. Clin. Oncol. 34 (2016) 2761–2768.
[21] L. Cortes-Dericks, G.L. Carboni, R.A. Schmid, G. Karoubi, Putative cancer stem cells in malignant pleural mesothelioma show resistance to cisplatin and pemetrexed, Int. J. Oncol. 37 (2010) 437–444.
[22] M. Vandamme, E. Robert, S. Lerondel, V. Sarron, D. Ries, S. Dozias, J. Sobilo, D. Gosset, C. Kieda, B. Legrain, J.M. Pouvesle, A.L. Pape, ROS implication in a new antitumor strategy based on non-thermal plasma, Int. J. Cancer 130 (2012) 2185–2194.
[23] H. Tanaka, M. Mizuno, K. Ishikawa, H. Kondo, K. Takeda, H. Hashizume, K. Nakamura, F. Utsumi, H. Kajiyama, H. Kano, Y. Okazaki, S. Toyokuni, S. Akiyama, S. Maruyama, S. Yamada, Y. Kodera, H. Kaneko, H. Terasaki, H. Hara, T. Adachi, M. iida, I. Yajima, M. Kato, F. Kikkawa, M. Hori, Plasma with high electron density and plasma-activated medium for cancer treatment, Clin. Plasma Med. 3 (2015) 72–76.
[24] S. Toyokuni, The origin and future of oxidative stress pathology: from the recognition of carcinogenesis as an iron addiction with ferroptosis-resistance to non-thermal plasma therapy, Pathol. Int. 66 (2016) 245–259.
[25] S. Kalghatgi, C.M. Kelly, E. Cerchar, B. Torabi, O. Alekseev, A. Fridman, G. Friedman, J. Azizkhan-Clifford, Effects of non-thermal plasma on mammalian cells, PLoS One 6 (2011) 1–11.
[26] T. Kaneko, S. Sasaki, K. Takashima, M. Kanzaki, Gas-liquid interfacial plasmas producing reactive species for cell membrane permeabilization, J. Clin. Biochem. Nutr. 60 (2017) 3–11.
[27] J.-S. Chang, Recent development of plasma pollution control technology: a critical review, Sci. Technol. Adv. Mater. 2 (2001) 571–576.
[28] J.D. Harper, N.A. Charipar, C.C. Mulligan, X. Zhang, R.G. Cooks, Z. Ouyang, Low-temperature plasma probe for ambient desorption ionization, Anal. Chem. 80 (2008) 9097–9104.
[29] E. Stoffels, I.E. Kieft, R.E.J. Sladek, L.J.M. v.d. Bedem, E.P. v.d. Laan, M. Steinbuch, Plasma needle for in vivo medical treatment: recent developments and perspectives, Plasma Sources Sci. Technol. 15 (2006) S169–S180.
[30] M.G. Kong, G. Kroesen, G. Morfill, T. Nosenko, T. Shimizu, J. van Dijk, J.L. Zimmermann, Plasma medicine: an introductory review, New J. Phys. 11 (2009) 115012.
[31] G. Fridman, A. Shereshevsky, M.M. Jost, A.D. Brooks, A. Fridman, A. Gutsol, V. Vasilets, G. Friedman, Floating electrode dielectric barrier discharge plasma in air promoting apoptotic behavior in melanoma skin cancer cell lines, Plasma Chem. Plasma Process. 27 (2007) 163–176.
[32] L. Shi, Y. Wang, F. Ito, Y. Okazaki, H. Tanaka, M. Mizuno, M. Hori, D.R. Richardson, S. Toyokuni, Biphasic effects of l-ascorbate on the tumoricidal activity of non-thermal plasma against malignant mesothelioma cells, Arch. Biochem. Biophys. 605 (2016) 109–116.
[33] Y. Okazaki, Y. Wang, H. Tanaka, M. Mizuno, K. Nakamura, H. Kajiyama, H. Kano, K. Uchida, F. Kikkawa, M. Hori, S. Toyokuni, Direct exposure of non-equilibrium atmospheric pressure plasma confers simultaneous oxidative and ultraviolet modifications in biomolecules, J. Clin. Biochem. Nutr. 55 (2014) 207–215.
[34] M. Vandamme, E. Robert, S. Pesnel, E. Barbosa, S. Dozias, J. Sobilo, S. Lerondel, A. Le Pape, J.-M. Pouvesle, Antitumor effect of plasma treatment on U87 glioma xenografts: preliminary results, Plasma Process. Polym. 7 (2010) 264–273.
[35] H. Tanaka, M. Mizuno, K. Ishikawa, K. Nakamura, H. Kajiyama, H. Kano, F. Kikkawa, M. Hori, Plasma-activated medium selectively kills glioblastoma brain tumor cells by down-regulating a survival signaling molecule, AKT kinase, Plasma Med. 1 (2011) 265–277.
[36] S.Y. Kim, H.J. Kim, S.U. Kang, Y.E. Kim, J.K. Park, Y.S. Shin, Y.S. Kim, K. Lee, C.H. Kim, Non-thermal plasma induces AKT degradation through turn-on the MUL1 E3 ligase in head and neck cancer, Oncotarget 6 (2015) 33382–33396.
[37] S. Iseki, K. Nakamura, M. Hayashi, H. Tanaka, H. Kondo, H. Kajiyama, H. Kano, F. Kikkawa, M. Hori, Selective killing of ovarian cancer cells through induction of apoptosis by nonequilibrium atmospheric pressure plasma, Appl. Phys. Lett. 100 (2012) 113702.
[38] M. Niwa, T. Hirayama, K. Okuda, H. Nagasawa, A new class of high-contrast Fe(II) selective fluorescent probes based on spirocyclized scaffolds for visualization of intracellular labile iron delivered by transferrin, Org. Biomol. Chem. 12 (2014) 6590–6597.
[39] J. Thiery, D. Keefe, S. Boulant, E. Boucrot, M. Walch, D. Martinvalet, S. Goping, R.C. Bleackley, T. Kirchhausen, J. Lieberman, Perforin pores in the endosomal membrane trigger the release of endocytosed granzyme B into the cytosol of target cells, Nat. Immunol. 12 (2011) 770–777.
[40] F.-T. Mu, J.M. Callaghan, O. Steele-Mortimer, H. Stenmark, R.G. Parton, P.L. Campbell, J. McCluskey, J.-P. Yeo, E.P. Tock, B.-H. Toh, EEA1, an early endosome-associated protein. EEA1 is a conserved α-helical peripheral membrane protein flanked by cysteine "fingers" and contains a calmodulin-binding IQ motif, J. Biol. Chem. 270 (1995) 13503–13511.
[41] S. Toyokuni, S. Okada, S. Hamazaki, M. Fujioka, J.-L. Li, O. Midorikawa, Cirrhosis of the liver induced by cupric nitrilotriacetate in Wistar rats: an experimetnal model of copper toxicosis, Am. J. Pathol. 134 (1989) 1263–1274.
[42] S. Kalghatgi, G. Friedman, A. Fridman, A.M. Clyne, Endothelial cell proliferation is enhanced by low dose non-thermal plasma through fibroblast growth factor-2 release, Ann. Biomed. Eng. 38 (2010) 748–757.
[43] J.W. Chang, S.U. Kang, Y.S. Shin, K.I. Kim, S.J. Seo, S.S. Yang, J.S. Lee, E. Moon, K. Lee, C.H. Kim, Non-thermal atmospheric pressure plasma inhibits thyroid papillary cancer cell invasion via cytoskeletal modulation, altered MMP-2/-9/uPA activity, PLoS One 9 (2014) e92198.
[44] S. Wilhelm, I. Collier, B. Marmer, A. Eisen, G. Grant, G. Goldberg, SV40-transformed human lung fibroblasts secrete a 92-kDa type IV collagenase which is identical to that secreted by normal human macrophages, J. Biol. Chem. 264 (1989) 17213–17221.
[45] M. Markman, D. Kelsen, Efficacy of cisplatin-based intraperitoneal chemotherapy as treatment of malignant peritoneal mesothelioma, J. Cancer Res. Clin. Oncol. 118 (1992) 547–550.
[46] N. Kaushik, N. Uddin, G.B. Sim, Y.J. Hong, K.Y. Baik, C.H. Kim, S.J. Lee, N.K. Kaushik, E.H. Choi, Responses of solid tumor cells in DMEM to reactive oxygen species generated by non-thermal plasma and chemically induced ROS systems, Sci. Rep. 5 (2015) 8587.
[47] W. Koppenol, The centennial of the Fenton reaction, Free Radic. Biol. Med. 15 (1993) 645–651.
[48] J.P. Kehrer, The Haber–Weiss reaction and mechanisms of toxicity, Toxicology 149 (2000) 43–50.
[49] D.R. Richardson, E. Baker, Two mechanisms of iron uptake from transferrin by melanoma cells. The effect of desferrioxamine and ferric ammonium citrate, J. Biol. Chem. 267 (1992) 13972–13979.
[50] D.R. Richardson, K. Milnes, The potential of iron chelators of the pyridoxal isonicotinoyl hydrazone class as effective antiproliferative agents II: the mechanism of action of ligands derived from salicylaldehyde benzoyl hydrazone and 2-hydroxy-1-naphthylaldehyde benzoyl hydrazone, Blood 89 (1997) 3025–3038.
[51] D. Richardson, E. Tran, P. Ponka, The potential of iron chelators of the pyridoxal isonicotinoyl hydrazone class as effective antiproliferative agents, Blood 86 (1995) 4295–4306.
[52] A. Linley, B. Valle-Argos, A.J. Steele, F.K. Stevenson, F. Forconi, G. Packham, Higher levels of reactive oxygen species are associated with anergy in chronic lymphocytic leukemia, Haematologica 100 (2015) e265–e268.
[53] B. Kalyanaraman, B.P. Dranka, M. Hardy, R. Michalski, J. Zielonka, HPLC-based monitoring of products formed from hydroethidine-based fluorogenic probes – the ultimate approach for intra- and extracellular superoxide detection, Biochim. Biophys. Acta 1840 (2014) 739–744.
[54] P.R. Angelova, M.H. Horrocks, D. Klenerman, S. Gandhi, A.Y. Abramov, M.S. Shchepinov, Lipid peroxidation is essential for alpha-synuclein-induced cell death, J. Neurochem. 133 (2015) 582–589.
[55] A. Wojtala, M. Bonora, D. Malinska, P. Pinton, J. Duszynski, M.R. Wieckowski, Methods to monitor ROS production by fluorescence microscopy and fluorometry, Methods Enzymol. 542 (2014) 243–262.
[56] A.E. Dikalova, A.T. Bikineyeva, K. Budzyn, R.R. Nazarewicz, L. McCann, W. Lewis, D.G. Harrison, S.I. Dikalov, Therapeutic targeting of mitochondrial superoxide in hypertension, Circ. Res. 107 (1) (2010) 106–116.
[57] G.P. Drummen, L.C. van Liebergen, J.A. Op den Kamp, J.A. Post, C11-BODIPY 581/591, an oxidation-sensitive fluorescent lipid peroxidation probe: (micro) spectroscopic characterization and validation of methodology, Free Radic. Biol. Med. 33 (2002) 473–490.
[58] D. Richardson, P. Ponka, The molecular mechanisms of the metabolism and transport of iron in normal and neoplastic cells, Biochim. Biophys. Acta 1331 (1997) 1–40.
[59] A.M. Thomson, J.T. Rogers, P.J. Leedman, Iron-regulatory proteins, iron-responsive elements and ferritin mRNA translation, Int. J. Biochem. Cell Biol. 31 (1999) 1139–1152.
[60] M. Hentze, L. Kuhn, Molecular control of vertebrate iron metabolism: mRNA-based regulatory circuits operated by iron, nitric oxide, and oxidative stress, Proc. Natl. Acad. Sci. USA 93 (1996) 8175–8182.
[61] J.-C. Drapier, H. Hirling, J. Wietzerbin, P. Kaldy, L. Kühn, Biosynthesis of nitric oxide activates iron regulatory factor in macrophages, EMBO J. 12 (1993) 3643–3649.
[62] D. Richardson, V. Neumannova, E. Nagy, P. Ponka, The effect of redox-related species of nitrogen monoxide on transferrin and iron uptake and cellular proliferation of erythroleukemia (K562) cells, Blood 86 (1995) 3211–3219.
[63] C. Bouton, M. Raveau, J.-C. Drapier, Modulation of iron regulatory protein functions further insights into the role of nitrogen- and oxygen-derived reactive species, J. Biol. Chem. 271 (1996) 2300–2306.
[64] S. Wardrop, D. Richardson, The effect of intracellular iron concentration and

nitrogen monoxide on Nramp2 expression and non-transferrin-bound iron uptake, Eur. J. Biochem. 263 (1999) 41–50.
[65] N. Akizu, V. Cantagrel, M.S. Zaki, L. Al-Gazali, X. Wang, R.O. Rosti, E. Dikoglu, A.B. Gelot, B. Rosti, K.K. Vaux, E.M. Scott, J.L. Silhavy, J. Schroth, B. Copeland, A.E. Schaffer, P.L. Gordts, J.D. Esko, M.D. Buschman, S.J. Field, G. Napolitano, G.M. Abdel-Salam, R.K. Ozgul, M.S. Sagiroglu, M. Azam, S. Ismail, M. Aglan, L. Selim, I.G. Mahmoud, S. Abdel-Hadi, A.E. Badawy, A.A. Sadek, F. Mojahedi, H. Kayserili, A. Masri, L. Bastaki, S. Temtamy, U. Muller, I. Desguerre, J.L. Casanova, A. Dursun, M. Gunel, S.B. Gabriel, P. de Lonlay, J.G. Gleeson, Biallelic mutations in SNX14 cause a syndromic form of cerebellar atrophy and lysosome-autophagosome dysfunction, Nat. Genet. 47 (2015) 528–534.
[66] J.D. Mancias, L.P. Vaites, S. Nissim, D.E. Biancur, A.J. Kim, X. Wang, Y. Liu, W. Goessling, A.C. Kimmelman, J.W. Harper, Ferritinophagy via NCOA4 is required for erythropoiesis and is regulated by iron dependent HERC2-mediated proteolysis, Elife 4 (2015) e10308.
[67] S. Sahni, D.H. Bae, P. Jansson, D.R. Richardson, The mechanistic role of chemically diverse metal ions in the induction of autophagy, Pharmacol. Res. 119 (2017) 118–127.
[68] N.A. Seebacher, D.J. Lane, P.J. Jansson, D.R. Richardson, Glucose modulation induces lysosome formation and increases lysosomotropic drug sequestration via the P-glycoprotein drug transporter, J. Biol. Chem. 291 (2016) 3796–3820.
[69] T. Kurz, A. Terman, U.T. Brunk, Autophagy, ageing and apoptosis: the role of oxidative stress and lysosomal iron, Arch. Biochem. Biophys. 462 (2007) 220–230.
[70] P.J. Jansson, T. Yamagishi, A. Arvind, N. Seebacher, E. Gutierrez, A. Stacy, S. Maleki, D. Sharp, S. Sahni, D.R. Richardson, Di-2-pyridylketone 4,4-dimethyl-3-thiosemicarbazone (Dp44mT) overcomes multidrug resistance by a novel mechanism involving the hijacking of lysosomal P-glycoprotein (Pgp), J. Biol. Chem. 290 (2015) 9588–9603.
[71] E.M. Gutierrez, N.A. Seebacher, L. Arzuman, Z. Kovacevic, D.J. Lane, V. Richardson, A.M. Merlot, H. Lok, D.S. Kalinowski, S. Sahni, P.J. Jansson, D.R. Richardson, Lysosomal membrane stability plays a major role in the cytotoxic activity of the anti-proliferative agent, di-2-pyridylketone 4,4-dimethyl-3-thiosemicarbazone (Dp44mT), Biochim. Biophys. Acta 1863 (7 Pt A) (2016) 1665–1681.
[72] M.P. D'Souza, J.T. August, A kinetic analysis of biosynthesis and localization of a lysosome-associated membrane glycoprotein, Arch. Biochem. Biophys. 249 (1986) 522–532.
[73] L. Yu, C.K. McPhee, L. Zheng, G.A. Mardones, Y. Rong, J. Peng, N. Mi, Y. Zhao, Z. Liu, F. Wan, Termination of autophagy and reformation of lysosomes regulated by mTOR, Nature 465 (2010) 942–946.
[74] E.L. Eskelinen, P. Saftig, Autophagy: a lysosomal degradation pathway with a central role in health and disease, Biochim. Biophys. Acta 2009 (1793) 664–673.
[75] D.J. Klionski, et al., Guidelines for the use and interpretation of assays for monitoring autophagy (3rd edition), Autophagy 12 (2016) 1–222.
[76] Y. Kabeya, N. Mizushima, T. Ueno, A. Yamamoto, T. Kirisako, T. Noda, E. Kominami, Y. Ohsumi, T. Yoshimori, LC3, a mammalian homologue of yeast Apg8p, is localized in autophagosome membranes after processing, EMBO J. 19 (2000) 5587–5941.
[77] N.F. Trincheri, C. Follo, G. Nicotra, C. Peracchio, R. Castino, C. Isidoro, Resveratrol-induced apoptosis depends on the lipid kinase activity of Vps34 and on the formation of autophagolysosomes, Carcinogenesis 29 (2008) 381–389.
[78] N. Mizushima, T. Yoshimori, B. Levine, Methods in mammalian autophagy research, Cell 140 (2010) 313–326.
[79] G. Napolitano, A. Ballabio, TFEB at a glance, J. Cell Sci. 129 (2016) 2475–2481.
[80] X. Zhang, X. Cheng, L. Yu, J. Yang, R. Calvo, S. Patnaik, X. Hu, Q. Gao, M. Yang, M. Lawas, MCOLN1 is a ROS sensor in lysosomes that regulates autophagy, Nat. Commun. 7 (2016) 12109.
[81] H.N. Ramanathan, Y. Ye, The p97 ATPase associates with EEA1 to regulate the size of early endosomes, Cell Res. 22 (2012) 346–359.
[82] M. Hamasaki, N. Furuta, A. Matsuda, A. Nezu, A. Yamamoto, N. Fujita, H. Oomori, T. Noda, T. Haraguchi, Y. Hiraoka, Autophagosomes form at ER-mitochondria contact sites, Nature 495 (2013) 389–393.
[83] D.J. Klionsky, E.-L. Eskelinen, V. Deretic, Autophagosomes, phagosomes, autolysosomes, phagolysosomes, autophagolysosomes… wait, I'm confused, Autophagy 10 (2014) 549–551.
[84] N. Mizushima, Autophagy: process and function, Genes Dev. 21 (2007) 2861–2873.
[85] R. Castino, N. Bellio, C. Follo, D. Murphy, C. Isidoro, Inhibition of PI3k class III-dependent autophagy prevents apoptosis and necrosis by oxidative stress in dopaminergic neuroblastoma cells, Toxicol. Sci. 117 (2010) 152–162.
[86] I. Tanida, N. Minematsu-Ikeguchi, T. Ueno, E. Kominami, Lysosomal turnover, but not a cellular level, of endogenous LC3 is a marker for autophagy, Autophagy 1 (2005) 84–91.
[87] C.H. Kim, J.H. Bahn, S.H. Lee, G.Y. Kim, S.I. Jun, K. Lee, S.J. Baek, Induction of cell growth arrest by atmospheric non-thermal plasma in colorectal cancer cells, J. Biotechnol. 150 (2010) 530–538.
[88] J.Y. Choi, H.M. Joh, J.M. Park, M.J. Kim, T.H. Chung, T.H. Kang, Non-thermal plasma-induced apoptosis is modulated by ATR- and PARP1-mediated DNA damage responses and circadian clock, Oncotarget 7 (2016) 32980–32989.
[89] S.U. Kang, J.H. Cho, J.W. Chang, Y.S. Shin, K.I. Kim, J.K. Park, S.S. Yang, J.S. Lee, E. Moon, K. Lee, C.H. Kim, Nonthermal plasma induces head and neck cancer cell death: the potential involvement of mitogen-activated protein kinase-dependent mitochondrial reactive oxygen species, Cell Death Dis. 5 (2014) e1056.
[90] M.G. Vander Heiden, L.C. Cantley, C.B. Thompson, Understanding the Warburg effect: the metabolic requirements of cell proliferation, Science 324 (2009) 1029–1033.
[91] J.C. Kwok, D.R. Richardson, The iron metabolism of neoplastic cells: alterations that facilitate proliferation? Crit. Rev. Oncol. Hematol. 42 (2002) 65–78.
[92] T.R. Daniels, T. Delgado, J.A. Rodriguez, G. Helguera, M.L. Penichet, The transferrin receptor part I: biology and targeting with cytotoxic antibodies for the treatment of cancer, Clin. Immunol. 121 (2006) 144–158.
[93] T.D. Oberley, L.W. Oberley, Antioxidant enzyme levels in cancer, Histol. Histopathol. 12 (1997) 525–535.
[94] S. Toyokuni, K. Okamoto, J. Yodoi, H. Hiai, Persistent oxidative stress in cancer, FEBS Lett. 358 (1995) 1–3.
[95] E. White, The role for autophagy in cancer, J. Clin. Invest. 125 (2015) 42–46.
[96] D.R. Richardson, D.S. Kalinowski, S. Lau, P.J. Jansson, D.B. Lovejoy, Cancer cell iron metabolism and the development of potent iron chelators as anti-tumour agents, Biochim. Biophys. Acta 2009 (1790) 702–717.
[97] D.R. Richardson, P. Ponka, E. Baker, The effect of the iron(III) chelator, desferrioxamine, on iron and transferrin uptake by the human malignant melanoma cell, Cancer Res. 54 (1994) 685–689.
[98] P.E. Starke, J.L. Farber, Ferric iron and superoxide ions are required for the killing of cultured hepatocytes by hydrogen peroxide, J. Biol. Chem. 260 (1984) 10099–10104.
[99] S. Josson, Y. Matsuoka, M. Gururajan, T. Nomura, W.C. Huang, X. Yang, J.T. Lin, R. Bridgman, C.Y. Chu, P.A. Johnstone, M. Zayzafoon, P. Hu, H. Zhau, D. Berel, A. Rogatko, L.W. Chung, Inhibition of beta2-microglobulin/hemochromatosis enhances radiation sensitivity by induction of iron overload in prostate cancer cells, PLoS One 8 (2013) e68366.
[100] S. Toyokuni, Iron-induced carcinogenesis: the role of redox regulation, Free Radic. Biol. Med. 20 (1996) 553–566.
[101] M.E. Hong, S.K. Hwang, W.S. Chang, B.W. Kim, J. Lee, S.J. Sim, Enhanced autotrophic astaxanthin production from Haematococcus pluvialis under high temperature via heat stress-driven Haber-Weiss reaction, Appl. Microbiol. Biotechnol. 99 (2015) 5203–5215.
[102] G. Cairo, L. Tacchini, G. Pogliaghi, E. Anzon, A. Tomasi, A. Bernelli-Zazzera, Induction of ferritin synthesis by oxidative stress, J. Biol. Chem. 270 (1995) 700–703.
[103] E.W. Müllner, L.C. Kühn, A stem-loop in the 3′ untranslated region mediates iron-dependent regulation of transferrin receptor mRNA stability in the cytoplasm, Cell 53 (1988) 815–825.
[104] F. Ito, T. Nishiyama, L. Shi, M. Mori, T. Hirayama, H. Nagasawa, H. Yasui, S. Toyokuni, Contrasting intra- and extracellular distribution of catalytic ferrous iron in ovalbumin-induced peritonitis, Biochem. Biophys. Res. Commun. 476 (2016) 600–606.
[105] G.M. Vercellotti, F.B. Khan, J. Nguyen, C. Chen, C.M. Bruzzone, H. Bechtel, G. Brown, K.A. Nath, C.J. Steer, R.P. Hebbel, J.D. Belcher, H-ferritin ferroxidase induces cytoprotective pathways and inhibits microvascular stasis in transgenic sickle mice, Front. Pharmacol. 5 (2014) 79.
[106] C. Settembre, C. Di Malta, V.A. Polito, M.G. Arencibia, F. Vetrini, S. Erdin, S.U. Erdin, T. Huynh, D. Medina, P. Colella, TFEB links autophagy to lysosomal biogenesis, Science 332 (2011) 1429–1433.
[107] A. Roczniak-Ferguson, C.S. Petit, F. Froehlich, S. Qian, J. Ky, B. Angarola, T.C. Walther, S.M. Ferguson, The transcription factor TFEB links mTORC1 signaling to transcriptional control of lysosome homeostasis, Sci. Signal. 5 (2012) ra42.
[108] N.A. Seebacher, D.R. Richardson, P.J. Jansson, Glucose modulation induces reactive oxygen species and increases P-glycoprotein-mediated multidrug resistance to chemotherapeutics, Br. J. Pharmacol. 172 (2015) 2557–2572.
[109] R. Scherz-Shouval, E. Shvets, E. Fass, H. Shorer, L. Gil, Z. Elazar, Reactive oxygen species are essential for autophagy and specifically regulate the activity of Atg4, EMBO J. 26 (2007) 1749–1760.
[110] E.I. Azzam, J.P. Jay-Gerin, D. Pain, Ionizing radiation-induced metabolic oxidative stress and prolonged cell injury, Cancer Lett. 327 (2012) 48–60.
[111] D. Kalamida, I.V. Karagounis, A. Giatromanolaki, M.I. Koukourakis, Important role of autophagy in endothelial cell response to ionizing radiation, PLoS One 9 (2014) 1–9.
[112] C. Ullio, U.T. Brunk, C. Urani, P. Melchioretto, G. Bonelli, F.M. Baccino, R. Autelli, Autophagy of metallothioneins prevents TNF-induced oxidative stress and toxicity in hepatoma cells, Autophagy 11 (2015) 2184–2198.